2016-01-01

Investigation On Pyroelectric Ceramic Temperature Sensors For Energy System Applications

Md Rashedul Hasan Sarker
University of Texas at El Paso, mhsarker@miners.utep.edu

INVESTIGATION ON PYROELECTRIC CERAMIC TEMPERATURE SENSORS FOR ENERGY SYSTEM APPLICATIONS

MD RASHEDUL HASAN SARKER

Doctoral Program of Mechanical Engineering

APPROVED:

Norman Love, Ph.D., Chair

Yirong Lin, Ph.D., Co-Chair

Ahsan Choudhuri, Ph.D.

David A. Roberson, Ph.D.

Charles Ambler, Ph.D.
Dean of the Graduate School

Dedication

To my parents, brothers and my wife.

INVESTIGATION ON PYROELECTRIC CERAMIC TEMPERATURE SENSORS FOR ENERGY SYSTEM APPLICATIONS

by

MD RASHEDUL HASAN SARKER, MS in Mechanical Engineering

DISSERTATION

Presented to the Faculty of the Graduate School of

The University of Texas at El Paso

in Partial Fulfillment

of the Requirements

for the Degree of

DOCTOR OF PHILOSOPHY

Department of Mechanical Engineering

THE UNIVERSITY OF TEXAS AT EL PASO

December 2016

ACKNOWLEDGEMENTS

This research was performed with the support of the U.S. Department of Energy Office of Fossil Energy at National Energy Technology Laboratory (NETL) under the HBCU/MI program with grant number of DEFE0011235. This work was also partially supported by the National Science Foundation (NSF) under NSF-PREM Grant No. DMR-1205302.

ABSTRACT

Temperature monitoring for energy generation systems plays an important role for control of overall safety and efficiency. To operate the energy system at optimum operating conditions, it is important to measure the real time temperature. Furthermore, harsh environment temperature sensing is desired since most sensors in energy systems are exposed to high temperature, high pressure, and corrosive environments. There is an increasing demand of wireless sensor networks and major interest in energy system applications for harsh environment and remote sensing applications. For this study, $LiNbO_3$ and $Pb(Zr_{0.52}Ti_{0.48})O_3$ (PZT) pyroelectric ceramic materials were used to develop temperature with wired and wireless connection respectively. Lithium niobate ($LiNbO_3$) has high Curie temperature (1210 °C), thus making it promising to be use as a sensor material for high temperature applications. A study was performed to actively measure the temperature up to 500 °C using a pyroelectric ceramic lithium niobate ($LiNbO_3$) as a sensor material. Different operating conditions were applied to the $LiNbO_3$ sample sensor including cyclic heating and cooling, low rate of temperature change, high rate of temperature change at low temperature ranges (<100 °C). For cyclic heating and cooling 2 mm and 1 mm thick $LiNbO_3$ sensors have shown 8 % and 6.7 % deviation respectively. For low and high rate of temperature changes with time, the $LiNbO_3$ sensor measured the temperature with 2% and 4% deviation, respectively. The $LiNbO_3$ sensor was also tested at high temperatures. Before high temperature measurement testing, the temperature dependent pyroelectric coefficient of $LiNbO_3$ was measured with a dynamic pyroelectric coefficient technique for different temperature ranges up to 500 °C. Temperature dependent pyroelectric coefficient of $LiNbO_3$ was found to be between -8.5 x 10^{-5} C/m^2 °C and -23.7 x 10^{-5} C/m^2 °C from room temperature to 500 °C. The $LiNbO_3$ sample sensor was then tested for higher temperatures and measured the temperature up to 220 °C, 280 °C, 410 °C and 500 °C with 4.31 %, 2.1 %, 0.4 % and 0.6% deviation, respectively. For developing a wireless temperature sensor, PZT ceramic material was used to measure the temperature for its higher signal strength with higher pyroelectric coefficient compare to $LiNbO_3$. An electromagnet was built with a pre-designed number of loops of wire, length, inner radius and outer radius. PZT sample was placed on top of a hot plate and it experienced maximum 0.84 °C/s rate of temperature change with time and maximum 4.59 µA current

was generated by the PZT due this corresponding rate of temperature change with time. Current from the PZT was supplied to the electromagnet to generate a magnetic field. Before using the PZT sample as a sensor, the electromagnet was characterized by measuring the magnetic field with a gaussmeter from different positions of the electromagnet including at the center, at the edge, at 1.27 cm, and 1.54 cm apart from the edge of the electromagnet along its axis. The gaussmeter was able to detect the magnetic field at the center, at the edge, at 1.24 cm, and 1.54 cm apart from the edge of the electromagnet with 11 %, 0.4 %, 11 %, and 0.9 % deviation, respectively. A nickel/iron/molybdenum alloy core material was also placed inside of the electromagnet to intensify the magnetic field strength by the factor of magnetic permeability of the core material. Gaussmeter measured the magnetic field 1.54 cm apart from the edge of the electromagnet along its axis with and without core material inside of the electromagnet. It was found that the electromagnet with core material intensified the magnetic field by a factor of two compared to the electromagnet without the core material. It was also found that the core material was experiencing induced magnetic field after removing current flow through the electromagnet. As the magnetic field was used to calculate the temperature of the PZT, the induced magnetic field on the core material was not desirable. After characterizing the magnetic field detection, the PZT sample and electromagnet without core material were prepared to measure the temperature wirelessly. For the wireless temperature measurement, two different temperatures (100 °C and 120 °C) were applied to the PZT ceramic material by placing it on top of a hot plate. The generated current was measured using a picoammeter and the generated magnetic field from the electromagnet was measured with a gaussmeter probe at 0.254 cm apart from the edge of the electromagnet. For two operating conditions (100 °C and 120 °C), the PZT sample was able to measure the temperature wirelessly with maximum 7.5 % and 4.3 % deviation from the theoretical temperature, respectively.

TABLE OF CONTENTS

LIST OF TABLES

LIST OF FIGURES

CHAPTER 1 INTRODUCTION AND BACKGROUND

1.1 Introduction

Temperature is one of the most important thermodynamic properties measured and controlled in energy generation systems. Continuous monitoring of real time temperature can lead to enhanced efficiency in these systems. This can be done by maintaining an optimum temperature that accommodates system safety parameters and maximize output[1]. Most components within an energy generation system including the coal gasification unit or gas turbine may experience high temperature (>1000 °C), high pressure and harsh environment. An accurate temperature probe capable of continuous monitoring in this harsh environment is critical to prevent structural and functional failure[2-4]. Few technologies are capable of withstanding continuous monitoring in this type of environment and are part of motivation of the current study.

The proper operation and management of energy systems will improve power consumption efficiencies and reduce the detrimental impact on the environment from emission of pollutants which includes green-house gases CO_2 and NO. There are different key parameters that control energy conversion technologies performance such as temperature and pressure along with other parameters such as flow rate and density. Among these, temperature is one of the most important parameters that controls the performance and efficiency of power generation systems. By maintaining an optimum temperature throughout the energy conversion process higher performance can be achieved. However, materials used in current power generation units have some practical limits that can cause catastrophic failure of components if exposed to too hot of a temperature. Due to this constraint, a temperature safety margin is maintained between high performance and reliability. The safety margin is met by obtaining the temperature lower than optimal temperature in order to avoid temperature induced fatigue failure. This safety margin becomes larger when operating temperature is not well characterized. However, safety margin can be minimize and achieve higher temperatures if real time temperature during the combustion

process is monitored. Hence, measurement of real time temperatures is a major area of research interest and considered as fundamental measurement parameter. Therefore, developing a temperature measurement method for a system while operating at harsh environment will be advantageous in reducing the safety margin.

1.2 Background

1.2.1 Temperature sensor

There are several methods available to measure the high temperature in a harsh environments including thermocouples, surface acoustic wave (SAW), optical sensors, microsensors and thermo-electric sensors. Typically thermocouple or thermo-electric sensors are the assembly of two different metal wires connected together and need to maintain hot and cold end. Using this method in harsh environment easily affected by noise and has limited life because of corrosive chemicals [2]. Optical sensors have significant advantages for measuring temperature dependent variables such as thermal radiation, thermal expansion coefficient and refractive index from material. Using this method is limited due to sensitivity and accuracy is affected by electromagnetic interference, radiation and corrosion [2]. To send and receive a signal from a sensor, a wired connection is typically used thus leading to high cost, design complexity and ultimately failure if exposed to a harsh environment. Therefore, research interests in wireless sensing have been increased. Wireless sensing technology requires built-in electronics like resistors, capacitors, batteries and other necessary components to receive and transfer wireless signals. Energy storage devices, power supplies, and other semiconductor materials are required for the development of wireless temperature sensing device which is highly vulnerable for harsh environment applications. Applications of wireless temperature sensing devices in energy conversion units with harsh environment like high pressure, high temperature and corrosive environment can cause damage to sensitive electronic materials eventually resulting in failure of components and measurement errors[5]. Therefore, further development of wireless sensing technology is required for operation in these harsh

environmental applications. To overcome the drawbacks of current sensor technologies, the proposed research project will present the development of low cost, self-powered wireless temperature sensing methods for the application of harsh environment in energy conversion units.

Monitoring processing parameters like temperature, pressure and flow rate in energy conversion unit are essential to improve performance and efficiency. The current work aims to develop a low cost, self-powered wireless temperature monitoring system for harsh environments found in energy systems. Various temperature measurement methods are available including a non-intrusive technique where the temperature is measured remotely without any point of contact from the heat source. The non-contact measurement method is essential when the point of measurement is in the harsh environment. On the other hand this technique is also essential to measure the temperature of a moving material without making any external housing on the system[6].

The most commonly used intrusive temperature measurement techniques are thermocouples and resistance thermometry with wide measurement ranges. However, they have limited life cycle for particular applications where they exposed to chemical reaction and erode due to long term exposure to the high temperature environment[7]. There are different types of non-intrusive temperature measurement methods including infrared thermometry, refractive index method, absorption and emission spectroscopy, spontaneous Rayleigh and Raman scattering method, optical temperature sensor and high temperature surface acoustic wave sensors. Infrared or radiation thermometry is a technique to measure temperature by monitoring thermal radiation in infrared spectrum and it is capable of measure temperature with wide range from 50 to 6000 K. This method is a non-contact measurement technique which can be explained with temperature and spectral radiance[6]. The refractive index method has also been used to measure temperature for compressible and incompressible flow of gases. Variation of flow velocity with changing density causes variation of the refractive index which is measurable. A relation can also be developed between the temperature and the variation in refractive index[8].

This is the most commonly used optical technique used to measure temperature from the variation of thermal radiation from the point of interest. This technique helps to measure localized temperature of an object [9]. Refraction index and thermal expansion coefficient also change with temperature that can be measure by the optical technique [10]. Sensitivity, accuracy and range is limited for commonly used optical temperature measurement technique due to electromagnetic interference and rotating components [2]. Surface acoustic wave (SAW) is also used as a passive sensor to measure temperature. An induced acoustic wave is passed through a piezoelectric material where the converted acoustic wave energy back as an electrical signal for temperature measurement [11]. Sardini E. *et al.* [12] proposed a method to measure 330 °C in harsh environment, by placing a hybrid MEMS inside the harsh environment temperature source and an external reading unit outside of the harsh environment.

1.2.2 Pyroelectric Material

Among various kinds of electric dipole moments in a dielectric material, a permanent electric dipole moment is formed by asymmetric distribution of unlike molecules. Materials with permanent electric moments are known as pyroelectric material or detector. This type of material exhibits a permanent electric dipole moment even in the absence of any external electric field. Ferroelectric and piezoelectric properties also exist in pyroelectric materials. One important parameter of pyroelectric detector is the pyroelectric coefficient (p). This coefficient can be described as the ratio of change in polarization (dP) and change in temperature (dT), where the unit is Coulomb/cm^{2}K

$$p = \frac{dP}{dT} \tag{1}$$

Primary and secondary pyroelectric coefficients are the two types of coefficient where primary coefficient is the result of temperature change and the secondary coefficient is due to the change in material volume with temperature. Ferroelectric materials have higher pyroelectric effects where the dipole moment can be reversed by applying an electric field[13]. All ferroelectric materials are pyroelectric materials but the opposite is not true. Another important

parameter of pyroelectric detectors is their Curie temperature (T_c). Dielectric properties and pyroelectric coefficient decreases with increasing temperature as the spontaneous polarization decreases as the Curie temperature is approached. Spontaneous polarization is zero at the Curie temperature of the material. Hence, Curie temperature plays an important role before selecting pyroelectric material or detector based on maximum temperature of operation.

There are different types of pyroelectric materials including crystals, polymers, and ceramics. Generally pyroelectric materials are high frequency thermal detectors with shorter thermal relaxation time and maximum response is obtainable at a time. The detector responsivity depends on its thermal response to the incident radiation and a response due to its temperature change (pyroelectric response). The thermal response of the detector elements depends on radiation absorption capacity and change in temperature due to absorbed radiation whereas the pyroelectric response due to change in temperature which is proportional to the pyroelectric coefficient[14-15]. Table 1.1 shows the Curie temperature and pyroelectric coefficient of pyroelectric materials at ambient temperature[16].

Table 1.1: List of Pyroelectric Materials and their Properties

Material	**Curie Temperature ($^{\circ}$C)**	**Pyroelectric Coefficient (10^{-8}CK^{-1}cm^{-2})**
Barium Titanate $BaTiO_3$	135	1.9
Lead Titanate, $PbTiO_3$	492	2.7
Lithium Niobate, $LiNbO_3$	1210	0.4
Lithium Tantalate, $LiTaO_3$	618	2.3
Lead Zirconate Titanate, PZT	365	4.7
PVC	100-266 (Melting Point)	0.01
Polyvinylidene Fluoride, PVDF	177 (Melting Point)	11

It is very important to choose a suitable pyroelectric material for different applications as every type of material has its own advantages and disadvantages. Following factors are considered before selecting a pyroelectric material[16].

a) Figure of Merit
b) Detector size
c) Range of operating temperature
d) Maximum temperature of operation and
e) Durability and availability

Selecting a proper pyroelectric material is very critical by considering their properties for different applications. Among various types of pyroelectric materials including nanowires[17], thin film[18] and bulk ceramics[19], where bulk ceramics shows higher pyroelectric properties with high coefficient and low self-discharging. High self-discharging is due to high specific surface area of the material that causes charge loss and low pyroelectric coefficient. Therefore, a bulk ceramic was used for the proposed work. For harsh environment applications, like high temperature and highly corrosive environments, a range of operating temperature and maximum operational temperature of pyroelectric ceramic is limited due to its Curie temperature. Materials lose pyroelectric properties when they heated above their Curie temperature[**Error! Bookmark ot defined.**]. Based on Curie temperature and pyroelectric coefficient, Lithium Niobate LNB ($LiNbO_3$) was selected for the proposed work because of sustainability in harsh environment. Unlike thermoelectric materials which requires hot and cold ends, the pyroelectric ceramic $LiNbO_3$ can be exposed to the harsh environment and subsequently results in a low cost and simple sensor design. $LiNbO_3$ was used to develop the temperature sensor with a wire connection. Lead zirconate titanate (PZT) on the other hand a ceramic material with higher pyroelectric coefficient compare to LNB but with lower Curie temperature. For wireless temperature sensor development, PZT ceramic material was used for this project due to its higher pyroelectric coefficient.

1.2.3 Pyroelectricity

Pyroelectricity is a property of certain type of materials which exhibits strong temperature variation dependence spontaneous polarization. The Pyroelectric effect can be described by the following Eq. (2)[16],

$$dp_i = p_i dT \tag{2}$$

Where p_i is the pyroelectric coefficient for change in polarization components (dP_i) with temperature change (dT). Spontaneous polarization (P_s) is the dipole moment per unit volume of the pyroelectric material where dipole moment is the unit cell of the material in the direction normal to the flat surfaces. In the absence of an electric field, the spontaneous polarization exists which is equivalent to the surface bound charge of the flat sample. Free charges like ions or electrons are attracted the flat surface of the sample, Figure 1.1(a). At constant temperature, if the electrode is attached to the top and bottom surface of the material with an ammeter having low resistance will experience no current flow due to constant P_s (Figure 1.1(b)). Increasing temperature of the material causes decrease of spontaneous polarization and also decreases of quantity in bound charge. The free charges started redistribute to compensate the decrease in bound charge and subsequently results a flow of current which is known as pyroelectric current, Figure 1.1(c). The current sign is reversed if the temperature decreases[20].

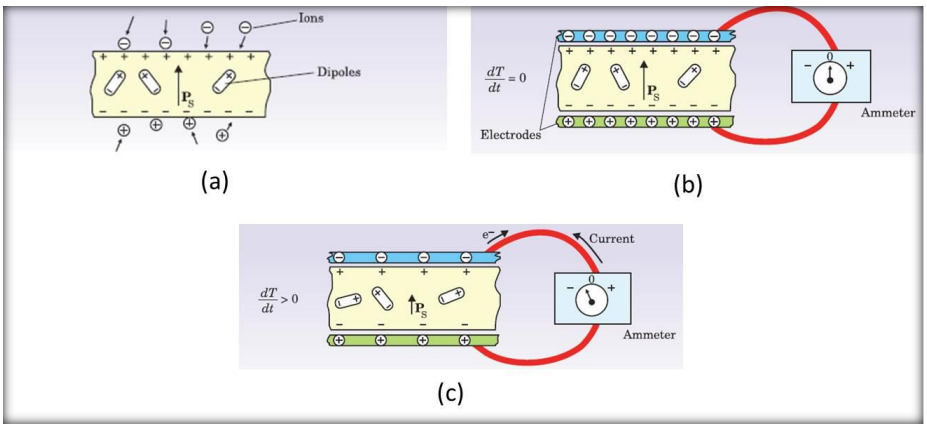

Figure 1.1: (a) Intrinsic dipole moment (b) Fashioned into a circuit with top and bottom electrode (c) Increased temperature with spontaneous polarization

The Pyroelectric effect is similar to the piezoelectric effect where mechanical stress is responsible for polarization. Pyroelectricity is also different from thermoelectricity where the Seebeck effect induced current is the result of temperature difference between hot and cold ends[21]. On the other hand, pyroelectricity is the result of change in temperature over time. The generated current is proportional to absolute temperature change. Therefore, to determine absolute temperature no reference temperature is needed. Pyroelectric properties from pyroelectric materials can used for different purposes including temperature measurement, energy harvesting, and laser energy meter[22-27].

With the change in temperature of the crystal in material, the net polarization is the dipole moment per unit volume and accumulated charge on the electrode of crystal surface is also proportional to per unit volume. No changes in temperature neutralize the charges by an internal depolarization field. Therefore, higher temperature change causes higher electric polarization with higher accumulation of charge on the electrode surface. Pyroelectric current can be defined from the accumulated charge on the electrode which is change in charge per unit time [14]. Generated current (I) through a homogenous pyroelectric material with temperature T at any time (t):

$$I = \frac{dQ}{dt} = \frac{dP_s}{dt} = -pA\frac{dT}{dt} \tag{3}$$

Here, Q is the charge, p is pyroelectric coefficient and A is the surface area of the electrode. By integrating Eq. (3), generated charge can be found[28]

$$Q = \int dQ = \int_{T_i}^{T_f} Idt = -pA(T_f - T_i) \tag{4}$$

Equation (4) describes that generated charge depends on temperature difference between initial and final temperature instead of rate of temperature change.

1.2.4 Pyroelectric Coefficient Measurement Techniques

Pyroelectricity measures the change of temperature by accumulating charge on planar capacitor structure[29]. According to the Eqs. (2) and (3), the generated charge and current from a pyroelectric detector is function of surface are of the detector (A), pyroelectric coefficient (p). Pyroelectric coefficient is also a function of temperature. To characterize the pyroelectric detector with respect to temperature, it is also important to determine the pyroelectric coefficient of the detector with respect to temperature. A quantitative value is necessary for the evaluation of pyroelectric material. Due to scarcity of turn-key equipment to measure the pyroelectric coefficient, there are several custom systems available to characterize the pyroelectric coefficient[30-31]. There are three different methods to determine the parameter using stimulus temperature including static, indirect and dynamic method[29]. Static method measures the total amount of pyroelectric charge with incremental increasing of temperature over a period of time. Equation (3) can be rewrite into following to calculate the pyroelectric coefficient.

$$p = \frac{1}{pA(T_f - T_i)} \int_{t_i}^{t_f} Idt = \frac{Q_f - Q_i}{pA(T_f - T_i)} \tag{5}$$

Q_f is the total amount of charge at time t_f and the Q_i is the initially measured charge at time t_i. This method is not widely used because over time the charges are compensated due to leakage current[29]. Indirect method measures the polarization (dP) to find out the pyroelectric coefficient using the following Eq. (6),

$$p = \frac{dP}{dT} \tag{6}$$

Indirect method is also not widely used due to possibility of incomplete switching of the polarization[29]. Dynamic methods are most widely used methods [32-36] to measure the pyroelectric coefficient using Byer-Roundy technique. This method uses Byer-Roundy technique[37] to measures the current from pyroelectric material by applying constant rate of temperature change with time (dT/dt) over a small range of temperature. A periodic cycle of heating and cooling with constant dT/dt is applied to the pyroelectric device to increase measurement accuracy. Pyroelectric device generates same amount of constant current for constant dT/dt with reverse polarity. The value of current for a constant dT/dt is taken to measure the pyroelectric coefficient using the following Eq. (7).

$$p = \frac{I}{A\frac{dT}{dt}} \tag{7}$$

1.2.5 Wireless Temperature Sensing

There is increasing demand of wireless sensor networks and has major interest in energy system applications for harsh environment and remote sensing applications. Sensing mechanism with wired connections increase the design complexity, costs and often required a separate housing to place the sensor and wired connections. Energy generation units like gas turbine, oxy-fuel combustion, gas-solid fluidized bed requires complicated sensing network to run the system efficiently. Wireless sensing systems can play an important role for such conditions. Wireless

systems can measure the parameters through most of the materials which minimize build separate housing and wire connections. Several methods applied to measure the temperature wirelessly including infrared thermometry, pyrometry, and surface acoustic wave (SAW) for high temperature applications. Thermometry and pyrometry use thermal radiation spectrum to measure the temperature[38]. SAW system measure the temperature from change in velocity of surface acoustic wave due to temperature change[39]. Most of the wireless temperature sensors in energy systems require battery power and they require periodic replacement which is costly and inconvenient for harsh environment applications [11],[40].

1.3 Overall Project Description

The overall project objective is to design, fabricate and demonstrate a low cost self-powered wireless temperature sensor that will generate current in response to temperature change. The sensing material has been chosen considering survivability in the harsh energy system. Pyroelectric properties of the sensing material are limited by their operating temperatures, as mentioned before. Sensing materials will lose their pyroelectric properties once they are heated above their Curie temperature. Lithium niobate, LNB ($LiNbO_3$) and Lead Zirconate Titanate (PZT) pyroelectric ceramic were selected for the proposed project to sense the temperature with wire connection and wireless connection respectively. Unlike thermoelectric material which requires a hot and cold end to measure relative temperature, a pyroelectric material can be exposed to the temperature source that leads to a simple and low cost sensor design.

The project was separated into two phases. The first phase of the project was to establish a method of temperature measurement by $LiNbO_3$ (LNB) ceramic material with wire connection at different operating condition up to 500 °C. The second phase of the project was to establish a wireless temperature measurement using lead zirconate titanate (PZT) ceramic material. LNB and PZT are both pyroelectric ceramic materials and generate current with respect to rate of temperature change with time. LNB has higher Curie temperature than PZT but lower

pyroelectric coefficient. Curie temperature dictates the feasibility of the ceramic material for different temperature range and pyroelectric coefficient dictates the response (current generation) of ceramic material with rate of temperature change with time.

For the first phase of the project, the sensing mechanism was based on the pyroelectric property of LNB that was exposed to a heated environment to accumulate charge on top and bottom surface of the material upon rate of temperature change with time. Two electrical wires were connected on top and bottom surfaces of the LNB material to measure the current with the help of a picoammeter. From measured current, the temperature experiencing by the LNB was found using Eq. (7)

For the second phase of the project, a PZT ceramic material with higher pyroelectric coefficient compare to LNB was selected. The generated charge carrying current due to rate of temperature change with time experiencing by the PZT was connected with a picoammeter and with an electromagnet in series connection. Picoammeter showed the amount of current passing through the electromagnet. Electromagnet generated magnetic field with respect to amount of current passed through it. The generated magnetic field from the electromagnet was measured by a gaussmeter remotely from a certain distance of 0.254 cm apart from the edge of the electromagnet. From the measured magnetic field, the temperature experiencing by the PZT was found wirelessly. Wireless temperature was measured up to 120 °C with PZT ceramic material. This project developed a new approach of temperature measurement method with pyroelectric ceramic material by wired connection and also by a passive wireless connection.

1.4 Objective

The goal of this project is to design, fabricate and demonstrate a low cost, self-powered wireless temperature sensor. This type of unit may someday be used in a full-scale energy conversion unit. The sensor will detect a magnetic field generated from a pyroelectric ceramic material due to experiencing temperature changes over time. The sensor, exposed to the high temperature environment, will transmit a wireless signal to a receiving unit. The receiving unit is

comprised of a gaussmeter which is used to detect magnetic field changes through various distance and materials.

A study will be conducted to have a thorough understanding of pyroelectric properties of ceramic material due to rate of temperature change with time. The pyroelectric materials generates current due to rate of temperature change with time. This pyroelectric current will be characterized at different operating conditions. The operation conditions include low rate of temperature changes, high rate of temperature changes, and a steady state conditions for prolonged time. A temperature sensor will be developed based on the pyroelectric properties of the ceramic material with wire connection.

The final stages of this project focus on receiving a wireless signal from a pyroelectric ceramic material that generates current due to experiencing temperature change with time. Generated current will be passed through an electromagnet to generate a magnetic field and will be detected by the wireless signal-receiving unit gaussmeter. Signals received by gaussmeter will be calibrated with the temperature change in pyroelectric ceramic for measurement of temperature.

CHAPTER 2 EXPERIMENTAL METHODOLOGY AND TECHNICAL APPROACHES

The project was divided into two phases. For the first phase, a proof-of-concept experiments was conducted to measure the temperature with a ceramic material. A commercial lithium niobate, LNB ($LiNbO_3$) ceramic material was used as a sensor material to measure the temperature for different operating conditions up to 500 °C. For the second phase of the project work, a lead zirconate titanate (PZT) ceramic material was used as sensor material for pyroelectric current source to generate magnetic field through an electromagnet. Generated magnetic field was then measured remotely with a gaussmeter. Remotely measured magnetic field was a function of rate of temperature change experiencing by the PZT.

2.1 First Phase Experiments

This section describes about the LNB sample sensor preparations, concept of temperature measurement using ceramic materials with wire connection and experimental methodologies to measure the temperature by the sample sensor at different operating conditions.

2.1.1 Sensor Sample Preparation

Two commercial lithium niobate ceramic materials (50.8 cm x 50.8 cm x 0.2 cm) and (50.8 cm x 50.8 cm x 0.1 cm) were purchased from Gooch & Housego, Palo Alto. Figure 2.1 shows the commercial LNB and Table 2.1 shows the physical properties of the LNB. A small section of 1 cm x 1 cm was cut from two different thicknesses of LNB and used as the sensor materials to measure the temperatures. Electrodes were placed on top and bottom surfaces of the sensor with a high temperature electrically and thermally conductive coating (Aremco, Pyro-Duct 597 C). A high temperature electrically and thermally conductive adhesive (Aremco, Pyro-Duct 597 A) was also used to connect two electrical leads on top and bottom surfaces of the sensor. The two electrical leads were then covered with high temperature ceramic sleeve (Mcmaster-Carr) to avoid any contact between the wires. Figure 2.2 shows the sample material of LNB, leads connection with adhesive, and high temperature ceramic sleeve.

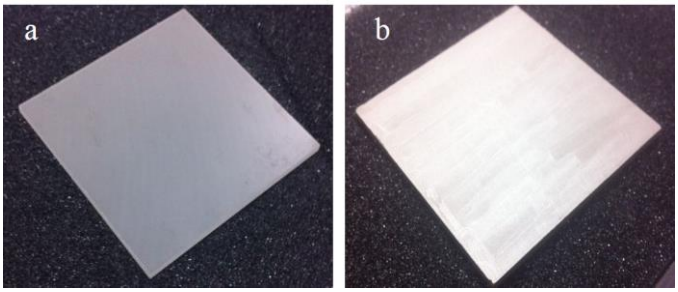

Figure 2.1: a) Commercial LNB b) High temperature resistive electrode on top and bottom surface

Table 2.1: Properties of commercial pyroelectric ceramic material

Dimension ($LiNbO_3$)	50.8×50.8cm×0.2cm 50.8×50.8cm×0.1cm
Density	4.65 g/cm^3
Curie Temperature	1142.3±0.7 ºC
Dielectric Constant (@ 25 ºC (unclamped <500 KHz)	ε_{11} = 85, ε_{33} = 28.7
Pyroelectric Coefficient (@ 25 ºC)	-8.3×10^{-5} C/ ºCm^2
Piezoelectric Strain Coefficients (@25 ºC ×10^{-12} C/N)	d_{12}=69.2 d_{31}=0.85 d_{22}=20.8 d_{33}=6.0
Thermal Conductivity (@ 25 ºC)	10^{-2} cal/cm.sec.ºC

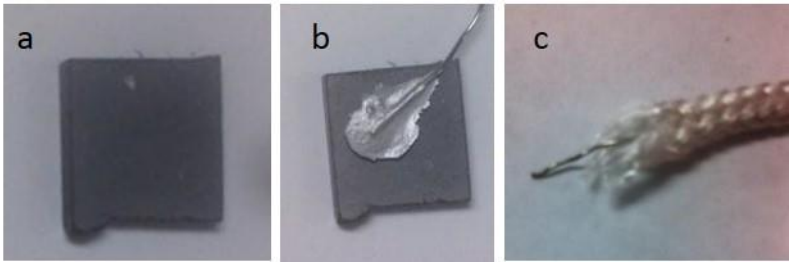

Figure 2.2: (a) $LiNbO_3$ sample (1 cmx1 cm) (b) Lead connection on top of $LiNbO_3$ (c) Ultra high temperature ceramic sleeve.

Resistance heating wire with nickel-chromium alloy (80 % Nickel & 20 % Chromium) was used as electrical leads (Omega Engineering, Omega NIC-80). Both coating and adhesive can withstand up to 927 ˚C, resistive heating wire can withstand 1150 ˚C, and the ultra-high temperature ceramic sleeve can withstand up to 1400 °C. The Curie temperature of the $LiNbO_3$

sensor (1210 ˚C) along with high temperature resistive coating, adhesive, electrical leads, and ceramic sleeve make an appropriate sensor setup to be used for high temperature applications. The two electrical leads were connected to a picoammeter (KEITHLEY 6485) to measure the current output from the sensor material once it experiences a rate of temperature change with time.

2.1.2 Temperature Measurement Experiments

For the first phase of experiments, temperature was measured from room temperature to 500 °C using the pyroelectric properties of a lithium niobate ($LiNbO_3$) ceramic. Lithium niobate is a pyroelectric material which has strong temperature variation dependent spontaneous polarization and loses its pyroelectric property when it is heated above its Curie temperature[13] Pyroelectric materials have been used as pyroelectric thermometer for low temperature applications and for monitoring indoor objects based on a pyroelectric infrared sensor thermometer[41],[42]. Among different types of pyroelectric material, lithium niobate has higher Curie temperature (1210 °C) than PZT and PVDF, which makes this material promising for high temperature measurement applications. Pyroelectricity is a phenomenon of certain materials showing temperature dependent spontaneous polarization. Both increasing and decreasing of temperature cause the changes in energy of atoms, crystal structure, and material polarity[43],[44]. During the change in temperature, the pyroelectric material polarity changing maintains a net polarization which is proportional to the charge per unit volume and these charges accumulate on the surface of the material[14].

Generated current (I) through a homogenous pyroelectric material with temperature T at any time (t) is presented in Eq. (8):

$$I = \frac{dQ}{dt} = -pA\frac{dT}{dt} \tag{8}$$

In Eq. (8), Q is the generated charge due to the temperature change, *p* is the pyroelectric coefficient, *A* is the electrode surface area and $\frac{dT}{dt}$ is the rate of temperature change with time of the material. By integrating Eq. (8) for a certain period of time the total amount of generated charge can be determined by Eq. (9) [28].

$$Q = \int_{t_i}^{t_f} I dt = \int_{t_i}^{t_f} -pA\frac{dT}{dt}dt = \int_{T_i}^{T_f} -pA dT = -pA(T_f - T_i) \tag{9}$$

Equation (9) shows that the generated charge depends on temperature difference between the initial and final temperature instead of rate of temperature change with time. Equation (9) can be rewritten into Eq. (10) to calculate the temperature of pyroelectric material at any specific time.

$$T_f = -\frac{1}{pA}\int_{t_i}^{t_f} I dt + T_i \tag{10}$$

Here T_i is the initial temperature of the pyroelectric ceramic material at time t_i, and T_f is the final temperature of the material at any specific time t_f. For most of the testing, the initial temperature (T_i) can be used as room temperature if the testing starts at room temperature. The pyroelectric coefficient (p), electrode area (A), initial temperature (T_i) and the total amount of current (I) generated by the material for a period of time (t_i to t_f) were used with Eq. 10 to calculate the final temperature (T_f). In this study, a $LiNbO_3$ sensor was placed in an environment so that it can experience different rates of temperature changes with time. To heat the $LiNbO_3$ sensor, a silicon heating pad, oven, and tube furnace were used. Once the $LiNbO_3$ sensor experience a rate of temperature change with time, the sensor generates a current. Numerical integration with Simpson's one third rule [45] was applied to calculate the total amount of current for any certain period of time ($\int_{t_i}^{t_f} I dt$) and the final temperature (T_f) of the $LiNbO_3$ sensor was calculated using Eq.10. Sarker et. al presented the results for low and high temperature

measurement using this technique from room temperature to 100 °C for both a heating and cooling cycle[46-47].

2.1.3 Pyroelectric Coefficient Measurement of LNB

Pyroelectric coefficient of LNB is also a function of temperature. The temperature dependence of pyroelectric coefficient has importance in the measurement of sensor temperature. The pyroelectric coefficient for LNB has been reported between -4.10 x 10-9 C/m^2 °C and (-6.4± 0.6) x 10-5 C/m^2°C [48]-[49]. Savage et al.[48] conducted dynamic pyroelectric measurement technique from 25 °C to 450 °C and the coefficients values were determined to be between -4.10 x 10-9 C/m^2 ° and -16.10 x 10^{-5} C/m^2 °C for this temperature range, respectively. The variation of the pyroelectric coefficient can be approximated using a nonlinear relation within this temperature range. This nonlinear dependence of pyroelectric coefficient of $LiNbO_3$ with temperature could be us in Eq. (10) to determine the instantaneous temperature of the sensor.

Although the non-linear relation of pyroelectric coefficient value as a function of temperature could be considered from Savage et al.[48], the value may vary according to LNB manufacturing processes. The difference of pyroelectric coefficient value at room temperature was found between Savage et al. sample of LNB and the sample of LNB commercially bought for this project. Due to this reason, a dynamic pyroelectric measurement technique was conducted with the sensor sample that was used for the current project to measure the pyroelectric coefficient with different increment of temperature ranges up to 500 °C. The pyroelectric coefficients of LNB at different temperature ranges measured by dynamic technique were used to find out the sensor temperature. An example of pyroelectric coefficient value measurement using dynamic technique at UTEP laboratory facility has shown in results and discussion section.

2.1.4 Temperature Measurement with LNB

The $LiNbO_3$ sensor was first subjected to characterize with heating and cooling. Small samples of $LiNbO_3$ (1 cm x 1 cm) with two different thicknesses (2 mm and 1 mm) were used

for this testing. Later, low and high rate of temperature changes with time were applied to the 2 mm thick sample sensor and temperatures were measured for these two different conditions in low temperature range (< 100 °C). These two experiments were conducted to test the readability of temperature by the $LiNbO_3$ sensor at a low temperature range (between room temperature to 100 °C) in different conditions, e.g. low rate of temperature change and high rate of temperature change with time. The pyroelectric coefficient (p) value of LNB was considered constant provided by the manufacturer at room temperature for low temperature ranges.

Temperature measurement with LNB at high temperature range (up to 500 °C) was also conducted with LNB. For high temperature measurement, temperature dependent pyroelectric coefficients were used to calculate the temperature.

2.1.4.1 Characterization of LNB with Heating and Cooling

In this experiment the generated current output of the LNB ceramic material due to heating and cooling was characterized. Small sample of LNB (1 cm x 1 cm) with two different thicknesses (2 mm and 1 mm) were used for this testing. A silicon-heating pad was used to apply a 14.5 W/cm^2 heat flux to the bottom of the sample for 210 s and then allowed to cool naturally for the following 300 s. An increasing rate of temperature change of the sample by silicon heating pad with 14.5 W/cm^2 heat flux was found for the first 210 s and then the rate of temperature change started to decrease and becomes near zero. Since the pyroelectric current is a function of rate of temperature change with time, during the heating cycle, the near zero rate of temperature change was not considered and then the cooling cycle started. The power supply to the heating pad was cut off after 210 s and the sample was allowed to cool naturally for the next 300 s and have a rate of temperature change with a negative slope and also have a near zero rate of temperature change at the end of cooling cycle. A K-type surface thermocouple was mounted on top of the sample. Under the same heating flux (14.5 W/cm^2); the sample with 2 mm thickness experienced a rate of temperature change as high as 0.5 °C/s and 0.3 °C/s during heating and cooling, respectively. The 1 mm thick sample experienced a rate of temperature

change as high as 0.62 °C/s and 0.4 °C/s during heating and cooling, respectively. Two electrical leads from the sample were connected with a picoammeter (KEITHLEY 6485) to measure the generated current from LNB with respect to rate of temperature change with time.

2.1.4.2 Temperature Measurement at a Low Rate of Temperature Change with LNB

For low rate of temperature change with time the LNB sensor was placed on top of a silicon heating pad. A surface thermocouple was mounted on top of the sensor to compare with temperature sensing reading from LNB. The sensor was subjected to experience temperature change from 22.50 °C to 27.75 °C within 650 s with an average rate of temperature change of 0.008 °C/s and maintained steady state condition for the next 700 s for steady state sensing characterization. As the sensor was experiencing very low rate of temperature change with time, a bottom surface thermocouple was not placed. A bottom surface thermocouple act as a thermal barrier between the heating pad and sensor. The difference between the bottom surface and top surface of the sensor is due to the thermal resistance of the sample. A sandwich structured sample with top and bottom surface thermocouple was investigated and the results are shown in results and discussion section. Figure 2.3 presents the schematic diagram of heating pad experimental setup for the low rate of temperature change with time for LNB sensor.

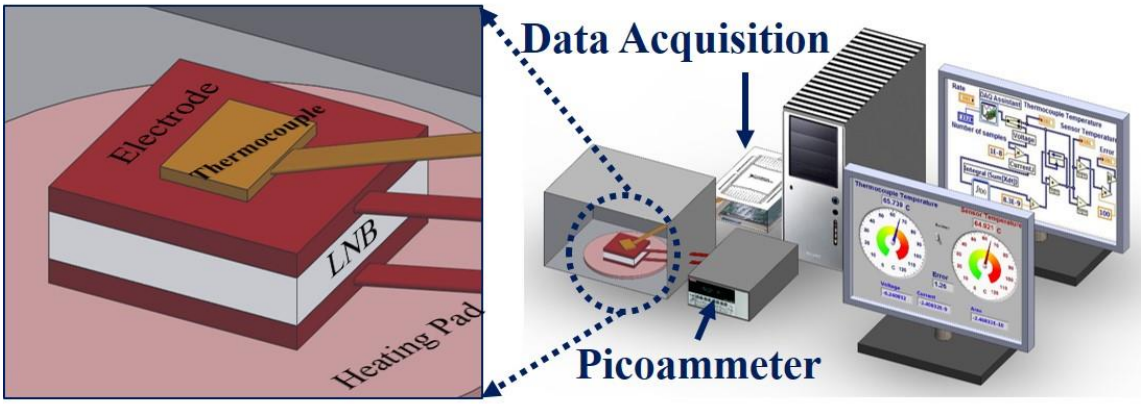

Figure 2.3: Schematic diagram of experimental setup for a low rate of temperature change with time for LNB sensor

2.1.4.3 Temperature Measurement at a High Rate of Temperature Change with LNB

For the high rate of temperature change with time experiment, an oven was set at 100 °C. Once the oven reached 100 °C, the LNB sensor was placed inside of the oven along with a surface thermocouple through a small opening in the oven. In this test, the LNB sensor experienced high rate of temperature change with time as the oven inside environment was already at 100 °C. The surface thermocouple reading reached 81 °C within 190 s with an average rate of temperature change 0.3 °C/s and remained steady state for the next 1600 s for steady state sensing characterization. Figure 2.4 presents the schematic diagram of the oven experimental setup for high rate of temperature change with time for LNB sensor

Figure 2.4: Schematic diagram of experimental setup for a high rate of temperature change with time for LNB sensor

2.1.4.4 Temperature Measurement at a High Range (up to 500 °C) with LNB

For the high temperature tests from room temperature to 500 °C, the LNB sensor was placed inside of a tube furnace (MTI Corporation, OTF-1200 X-S-UL), Figure 2.5. The temperature of the tube (5 cm diameter) furnace was set with the help of PID automatic control. The temperature can be set for 30 different programmable steps and reaches a maximum 0.33 ˚C/s heating rate. Experimental tests were done by setting the tube furnace temperature from room temperature to 500 ˚C with two different heating rates of 0.25 ˚C/s and 0.33 ˚C/s. A K-type thermocouple rod was also placed near the LNB sensor inside the tube furnace to compare with

temperature sensing reading from LNB. The two ends of the tube were open to the atmosphere to avoid any pressure built inside. The two electrical leads from the LNB sensor were connected to a picoammeter (KEITHLEY 6485) to measure the current output from the LNB. As the K-type thermocouple rod was placed near the LNB sensor, the temperature measured by the thermocouple was assumed to be the temperature profile of the LNB sensor instead of the set temperature of the tube furnace. The generated current from the LNB was used to calculate the temperature of the LNB sensor and compared with the temperature measured by the K-type thermocouple rod.

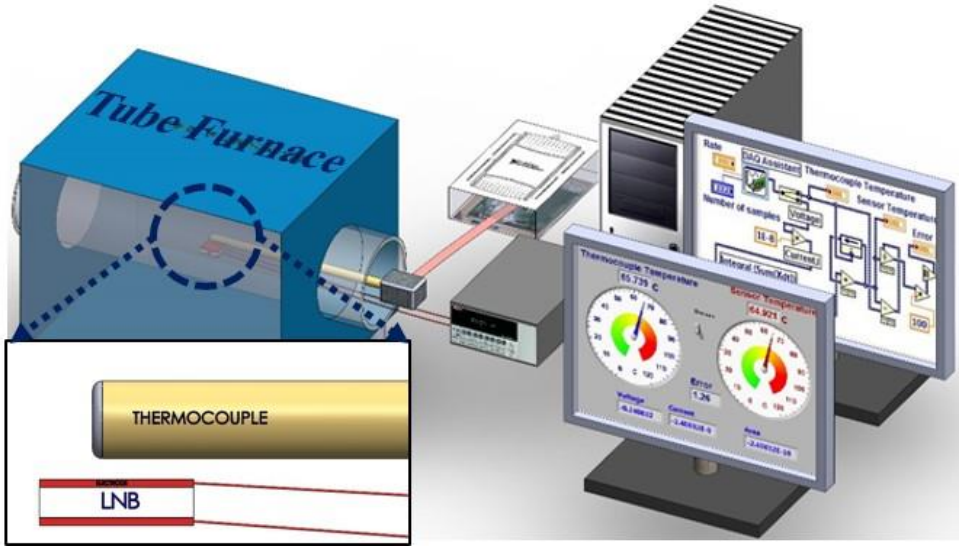

Figure 2.5: Schematic diagram of experimental setup for a high temperature test in tube furnace with LNB sensor.

2.2 Second Phase Experiments

This section describes the concept of temperature measurement in a wireless configuration. The sensing mechanism is based on the property of the pyroelectric ceramic that was exposed to a heat source and the pyroelectric ceramic generates charge upon the rate of temperature change with time. The generated charge carrying currents were passed through a conductive wire. A moving charge through a long straight wire can produce circular magnetic

field around the wire. The direction of magnetic field around a wire can be described by right hand rule. This magnetic field is the area around a current carrying wire where a force can be felt due to this field. Using a coil shape of wire (Electromagnet/Solenoid) instead of a straight wire increases the strength of the magnetic field for a given amount of current.

The proposed sensing method has a leads arrangement on the sensor that was connected to an electromagnet. Generated current from the sensor sample passed through the electromagnet and the electromagnet produced magnetic field at a magnitude proportional to the current. An external receiver (Gaussmeter) was placed at a certain distance of 0.254 cm from the edge of the electromagnet to detect the magnetic field wirelessly thus transferring the signal wirelessly to an external receiver. The electromagnet was made using university laboratory facilities by maintaining desired number of loops of wire and length. Figure 2.6 presents the concept of wireless temperature measurement technique with remote sensing device and signal processing unit outside of the harsh environment.

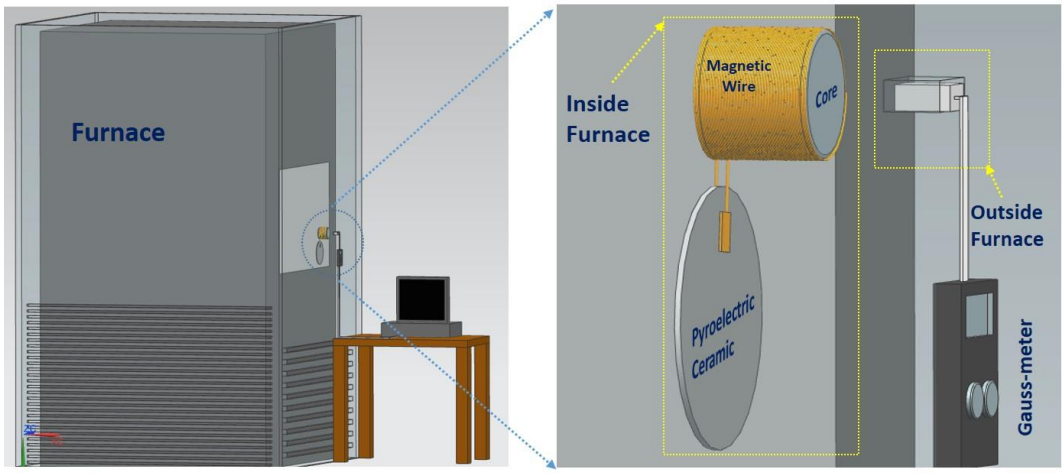

Figure 2.6: Schematic diagram of wireless temperature measurement technique with pyroelectric ceramic material

2.2.1 Magnetic Field of an Electromagnet

The magnetic field is a function of current supplied to the electromagnet, length, and number of turns of the wire. The relation between current and magnetic field at the center of an electromagnet can be described by the following Eq. (16),

$$B = \frac{\mu_0 NI}{L} \tag{11}$$

Where μ_0 is the magnetic permeability of free space, N is the number of loops of the wire, I is the supplied current to the electromagnet, and L is the length of the electromagnet. For a long electromagnet, the magnetic field at the edge of the electromagnet is half of the amount of center. Figure 2.7 presents a general form of an electromagnet with length L and radius R.

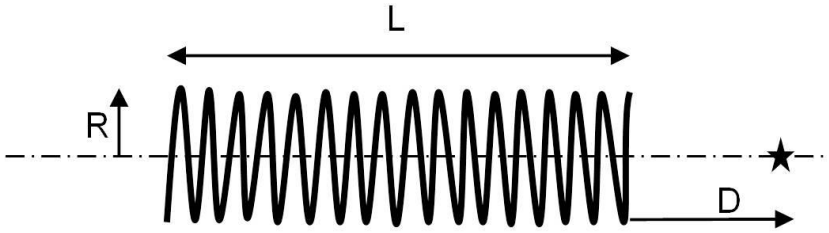

N= Number of turns
L= Length of the electromagnet
R= Radius of the electromagnet
D= Distance from the edge of the electromagnet along axis

Figure 2.7: Schematic diagram of an electromagnet with a single layer of winding wire

To find out the magnetic field at a certain distance from the edge of the electromagnet along the axis is defined by the following Eq. (12)

$$B = \frac{\mu_0 NI}{2L}\left[\frac{L+D}{[R^2+(L+D)^2]^{\frac{1}{2}}} - \frac{D}{(R^2+D^2)^{\frac{1}{2}}}\right] \tag{12}$$

The magnetic field can be increased by increasing the number of turns and supply of current and using a high permeability core material. The current supply from pyroelectric ceramic depends on the rate of temperature change with time which would be limited during the experiment. For the current scenario increasing the number of turns is the best choice for increasing the magnetic field. This is since increasing the number of turns within a certain length will increase the radius of electromagnet. Figure 2.8 presents a schematic diagram of a finite electromagnet.

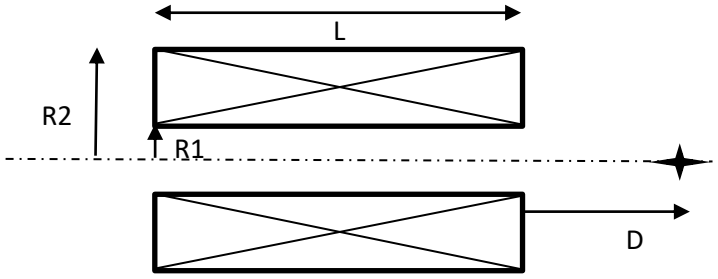

Figure 2.8 Schematic diagram of a general finite electromagnet

In this case, the magnetic field along the axis of an electromagnet in a certain distance is defined as following Eq. (13) by integrating over the radius,

$$B = \frac{\mu_0 NI}{2L(R_2 - R_1)}\left[(L+D)\ln\frac{\sqrt{R_2^2+(L+D)^2}+R_2}{\sqrt{R_1^2+(L+D)^2}+R_1} - D\ln\frac{\sqrt{R_2^2+D^2}+R_2}{\sqrt{R_1^2+D^2}+R_1}\right] \tag{13}$$

Here, D is the distance from the edge of the electromagnet. R_1 is the inner radius of the electromagnet and R_2 is the outer radius of the electromagnet after winding multiple turns within a length L.

2.2.2 Wireless Temperature Measurement Concept

For wireless temperature measurement, the magnetic field generated from the electromagnet with supplied current from pyroelectric ceramic was used. Magnetic fields were measured remotely with the help of a DC milligaussmeter (Alpha Lab Inc, Trifield).

In Eq. (13), current (I) is the only variable and others are physical properties of the electromagnet. Equation (13) can be rewritten as following Eq. (14) which leads to get the Eq. (15).

$$B = C \times I \tag{14}$$

$$I = \frac{B}{C} \tag{15}$$

Here, C is the constant found from multiplying all the physical parameters of the electromagnet including length, inner radius, outer radius, distance from the edge of the electromagnet, and magnetic permeability at free space. Equation (15) was placed into Eq. (10) to calculate the temperature wirelessly by measuring magnetic field from the following Eq. (16).

$$T_f = -\frac{1}{pA}\int_{t_i}^{t_f} I dt + T_i = -\frac{1}{pAC}\int_{t_i}^{t_f} B dt + T_1 \tag{16}$$

Here, T_f is the temperature experiencing by the pyroelectric material at any instantaneous time which is a function of magnetic field. Experimentally a linear relationship of magnetic fields was found from the center of the electromagnet to a certain distance along the axis from the edge of the electromagnet up to 0.254 cm. A comparison between experimental and analytical magnetic fields has also shown in results and discussion section.

2.2.3 Experimental Setup of Wireless Temperature Sensing

A 3D printed block was made with desired shape for winding the loops of wire around it with the help of university facilities. 30 gauge motor winding wire (McMaster-Carr) was winded around the block to make the electromagnet. Figure 2.9 presents the 3D printed block and the electromagnet. Physical parameters of the electromagnet is also presented in Table 2.2.

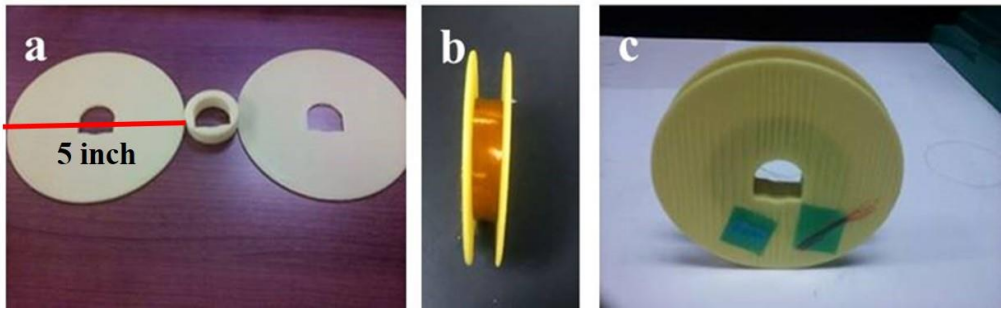

Figure 2.9: a) 3D printed block for electromagnet b) Top view of electromagnet, and c) Side view of electromagnet

Table 2.2: Physical parameters of the electromagnet

Number of Turn	6935
Length	1.27 cm
Inner Diameter	3.8 cm
Outer Diameter	7.4 cm
Magnetic wire	30 Gauge/ copper (enamel coated)

For wireless temperature measurement with a pyroelectric ceramic material, a 7.5 X7.5 cm with 0.25 mm thick PZT was used instead of LNB for higher signal strength. PZT has approximate five times higher pyroelectric coefficient (-40 x 10-5 C/m^2 °C) than a LNB (-8.5 x 10-5 C/m^2 °C) at room temperature. The PZT sample was placed on top of a hot plate. A surface thermocouple was also attached on top of the PZT. The generated current from the PZT due to experiencing rate of temperature change with time (dT/dt) was passed through the electromagnet. Before connecting the two leads from the PZT's top and bottom surfaces to the electromagnet, a picoammeter was also connected in series connection to measure the current passing through the electromagnet. A magnetic field measurement probe from a DC milligaussmeter was placed at different places of the electromagnet. The amount of magnetic field is a function of physical parameters of the electromagnet and the amount of current passing through it from the PZT. Analytically, the magnetic field can be calculated from Eq. (13). Figure 2.10 presents the schematic diagram of the experimental setup to measure the magnetic field at the center of the electromagnet.

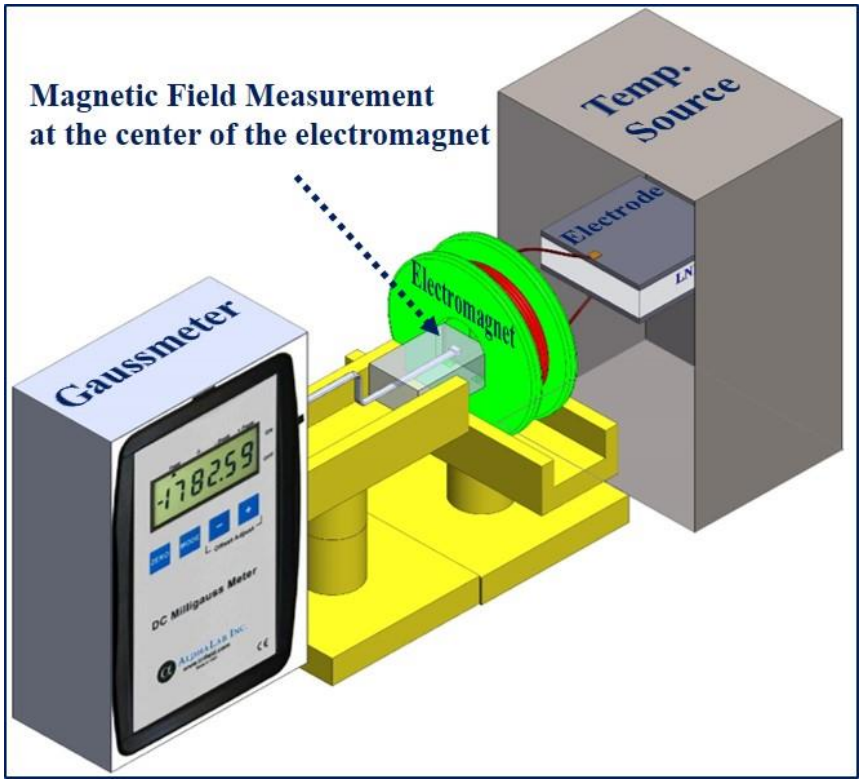

Figure 2.10: Magnetic field measurement at the center of the electromagnet

At first the magnetic field detection with the gaussmeter probe was characterized by placing the probe at the center, at the edge, at 1.27 cm apart from the edge and 1.54 cm apart from the edge of the electromagnet. When the probe was at 1.54 cm apart from the edge of the electromagnet, a nickel/iron/molybdenum alloy core material (Figure 2.11) was also placed inside of the 3D printed block to intensify the magnetic field from the electromagnet. The core material increase the magnetic field strength by a factor of magnetic permeability of the alloy material. Experimentally the magnetic permeability was measured for the alloy material.

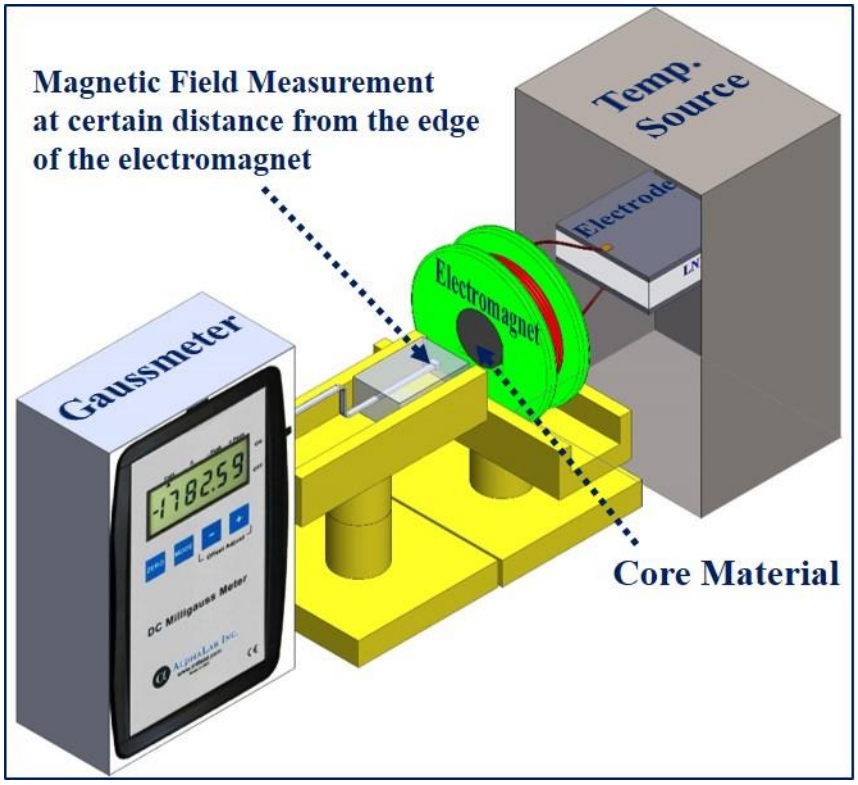

Figure 2.11: Magnetic field measurement at a certain distance from the edge of the electromagnet using an alloy core material

Once the magnetic field measurements were characterized by placing the gaussmeter probe at different positions, the temperature of the PZT sensor was measured wirelessly from the output of gaussmeter readings. The generated magnetic field due to current passing through the electromagnet was measured by a gaussmeter probe at 0.254 cm apart from the edge of the electromagnet. As the amount of current passing through the electromagnet was known by the picoammeter, a theoretical electromagnetic field was calculated using Eq. (13). This theoretical magnetic field was used to calculate the temperature of the PZT sensor using Eq. (16). This calculated temperature is the theoretical temperature of the PZT using theoretical magnetic field. The same current is passing through the electromagnet which generates magnetic field and measured with a gaussmeter probe at 0.254 cm apart from the edge of the electromagnet. This magnetic field is the experimental magnetic field and also used to calculate the temperature of

the PZT using Eq. (16). Both calculated temperature using theoretical magnetic field and experimental magnetic field were compared.

The DC milligaussmeter (Alpha Lab Inc, Trifield) used for this project was an improvement on the flux gate magnetometer that can measure magnetic field up to several times the strength of the Earth field. It has a resolution of 0.01 milligauss (1 nano-tesla) with a range of ±2000 milligauss (200 micro-tesla). The sensor on the gaussmeter probe was 'axial' that measured the magnetic field components in the same direction as it was pointed.

2.3 System Development for Temperature Measurement

A system was developed for testing and recording for experiments to measure the temperature using LabVIEW software and DAQ card from National Instruments (NI PCI-6221). Figure 2.12 presents an example setup to measure the temperature with LNB at low temperature range (< 100 °C). The LNB sample was placed on top of the silicon heating pad. The generated current from the LNB due to rate of temperature change with time was measured by the picoammeter.

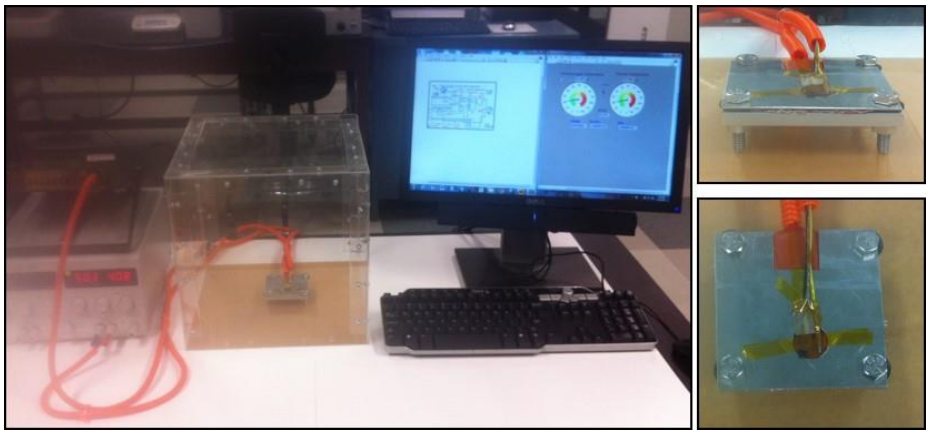

Figure 2.12: Experimental setup to measure the temperature at low temperature range (< 100 °C)

The input current to the picoammeter forced through a feedback resistor inside of the picoammeter and inverted analog output voltage from the operational amplifier was connected to the data acquisition board. The analog output voltage from the picoammeter was measured with

a LabVIEW VI set to a 500 Hz sampling rate using a data acquisition board. Later the voltage readings were converted to current value with a conversion factor provided by the picoammeter manufacturer. A program was written for the experiments which contain one switch to control the data recording. Figure 2.13 presents the program for temperature measurement that shows the thermocouple temperature and sensor temperature at the same time. DAQ assistant records two inputs with same rate and number of samples.

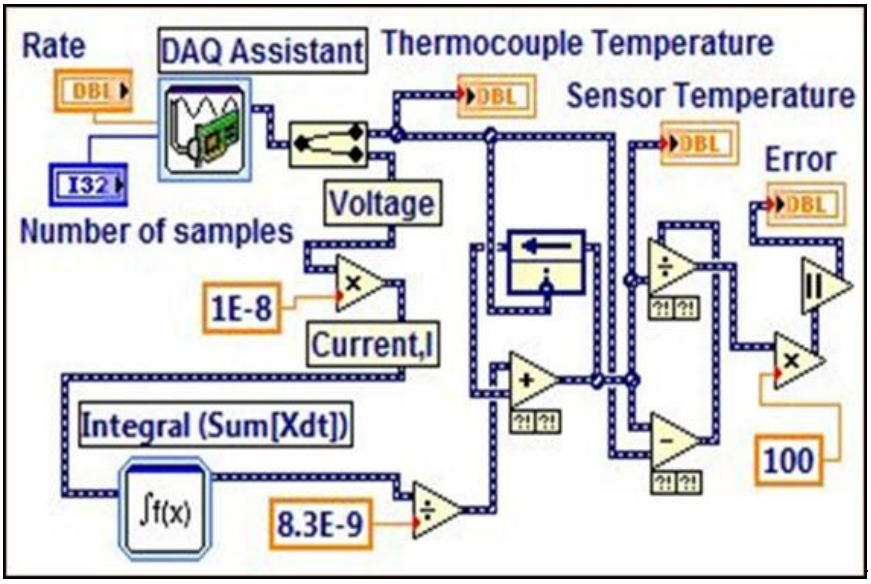

Figure 2.13: LabVIEW program

The first data input was the thermocouple temperature and the second data input was analog voltage output from the picoammeter. The program converted the voltage input into current value with a conversion factor. After conversion of analog voltage input into current output, the program perform the integral of current at every 0.002 s. This is the integral part from Eq. (10). After that the constant value of sensor electrode area and pyroelectric coefficient value were divided from the integral of current. The first initial temperature was taken from the thermocouple temperature input and after that the program always took the initial temperature from its previous calculated temperature and run in a loop configure to measure the temperature

over time from the sensor sample. Figure 2.14 shows the LabVIEW interface with thermocouple temperature and sample sensor temperature side by side with percentage of errors between them.

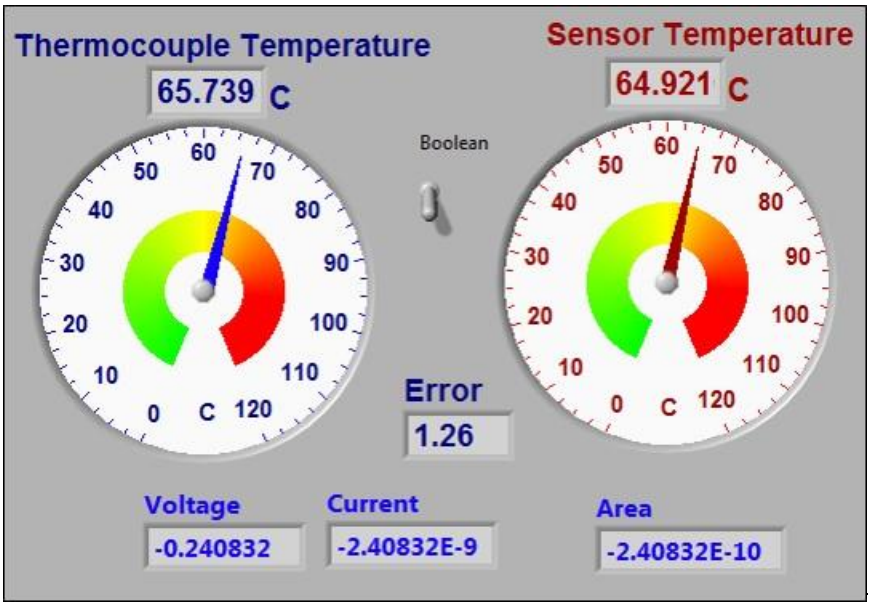

Figure 2.14: LabVIEW interface

2.4 Equipment

This section describes the specification of all the major equipment and devices used for the development of wired and wireless temperature sensor

2.4.1 Silicon Heating Pad

For heating the pyroelectric ceramic (Lithium Niobate) a commercial round shape silicone rubber fiberglass insulated flexible heater (Omega Engineering) was used. Figure 2.15 shows the image of the silicon heating pad with dimension of 3 inch diameter and 1.55 W/cm^2. The maximum capacity of the heater is 232^0 C. Pyroelectric ceramic was also placed inside of a furnace for heating with slow ramp of increasing temperature.

Figure 2.15: Silicon heating pad

2.4.2 Data Acquisition System

For system development of temperature sensing with wired connection the data was data was recorded via LabVIEW software with interface of a National Instrument data acquisition board NI PCI-6221. Figure 2.16 shows the acquisition system of NI PCI-6221. It has two 16-bit analog outputs with 24 digital I/O and 32-bit counters.

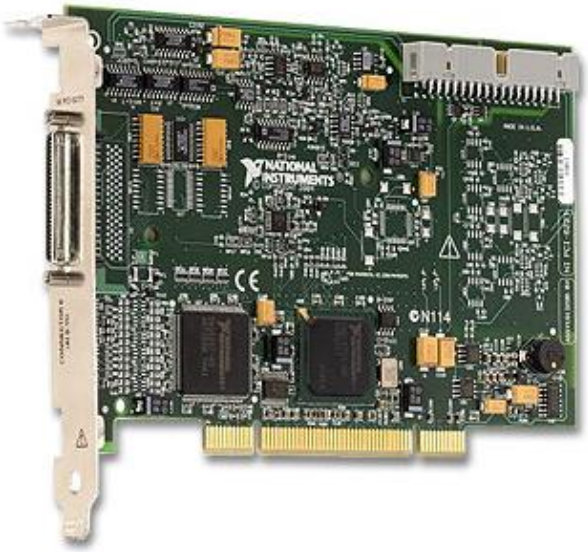

Figure 2.16: National instrument PCI-6221 data acquisition system

2.4.3 Tube Furnace

For high temperature measurements and temperature dependent pyroelectric coefficient measurements a tube furnace (MTI Corporation, OTF-1200 X-S-UL), Figure 2.17, was used. The temperature of the tube (5 cm diameter) furnace was set with the help of PID automatic control. The temperature can be set for 30 different programmable steps and reaches a maximum 0.33 ˚C/s heating rate.

Figure 2.17: National instrument PCI-6221 data acquisition system

2.4.4 Picoammeter

For all sensitive electrical measurement a picoammeter (KEITHLEY 6485) was used. This picoammeter was comprise with eight different current measurement ranges and high speed auto ranging options. The instrument was able to measure current from 200 fA to 20 mA at speeds up to 1000 readings per second. Figure 2.18 shows the picoammeter used for the project.

Figure 2.18: Picoammeter

CHAPTER 3 RESULTS AND DISCUSSIONS

The results from the 1st phase and 2nd phase experiments are presented in this chapter. The goal of the first phase experiments was to establish the feasibility and readability of lithium niobate, LNB ($LiNbO_3$) to measure temperature with wired connection at different operating conditions for low temperature range and for high temperature range up to 500 °C.

The second phase experiments sought to measure temperature wirelessly with pyroelectric ceramic material. For the wireless temperature measurements a lead zirconate titanate (PZT) ceramic was used for its higher pyroelectric coefficient compare to LNB. The results section shows the feasibility and readability of wireless temperature measurement with PZT at two different temperature ranges up to 100 °C.

3.1 First Phase Experimental Results

At first the sample sensor was tested to measure low temperature (<100 °C) for cyclic heating and cooling. Sensor samples with two different thicknesses (2 mm and 1mm) were tested in this condition. This test helped to identify the effects of sensor sample thickness. Sensor sample was also subjected to test for low and high rate temperature change with time for low temperature range (<100 °C). For low temperature range, the pyroelectric coefficient was considered constant provided by the LNB manufacturer. Later, sample sensor was subjected to test for high temperature range (up to 500 °C). For high temperature test, temperature dependent pyroelectric coefficients were considered. Temperature dependent pyroelectric coefficients were measured in UTEP laboratory facility for different temperature ranges.

3.1.1 Characterization of LNB with Heating and Cooling

Experimental results are shown here to determine the temperature from generated current of the pyroelectric ceramic material (LNB) with two different thicknesses. The temperature profiles and rates of temperature changes are shown for 2 mm and 1 mm thick samples in Figure 3.1.

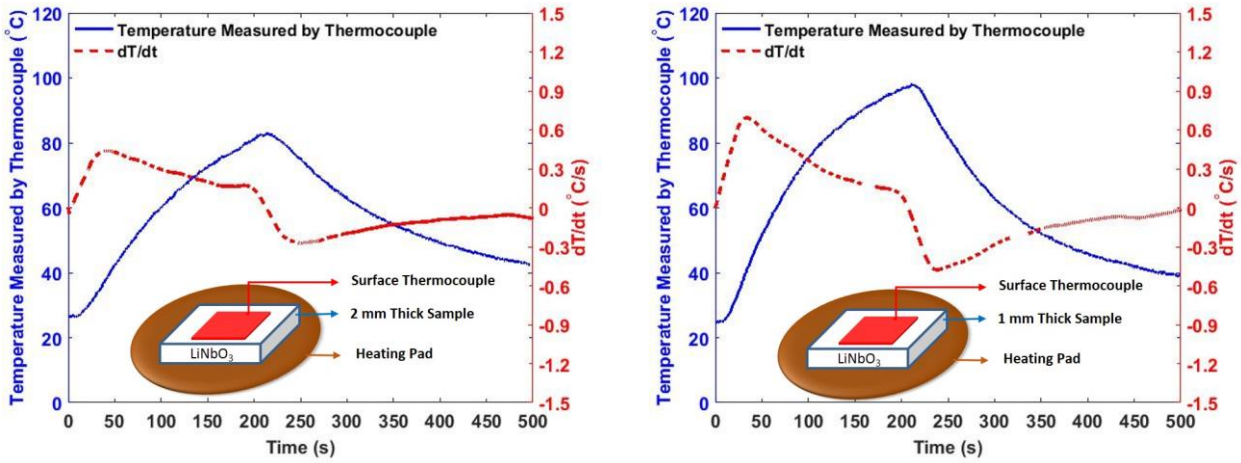

Figure 3.1: Temperature profile and rate of temperature change of the thermocouple mounted on top of the 2 mm and 1 mm thick $LiNbO_3$

In Figure 3.1 both the temperature profile and rate of temperature change with time show that the 1 mm thick sample reached a higher temperature with a higher rate of temperature change than the 2 mm thick sample for first 210 s of heating. The principles of conduction heat transfer states that for the same heat flow, cross sectional area, and material conductivity, the temperature difference between the surface in contact with the heating pad and top of the $LiNbO_3$ must be lower for a thinner sample [50]. Therefore, the thermocouple mounted on top of the sample measures a higher temperature for the 1 mm thick sample compared to the 2 mm thick sample. Figure 3.2 shows the current response with the rate of temperature change for both sample thicknesses. The pyroelectric coefficient and the area of the electrode are the same for both samples. As the thinner sample experiences a higher rate of temperature change ($\frac{dT}{dt}$), the 1 mm sample responds with a higher amount of current output than the 2 mm thick sample.

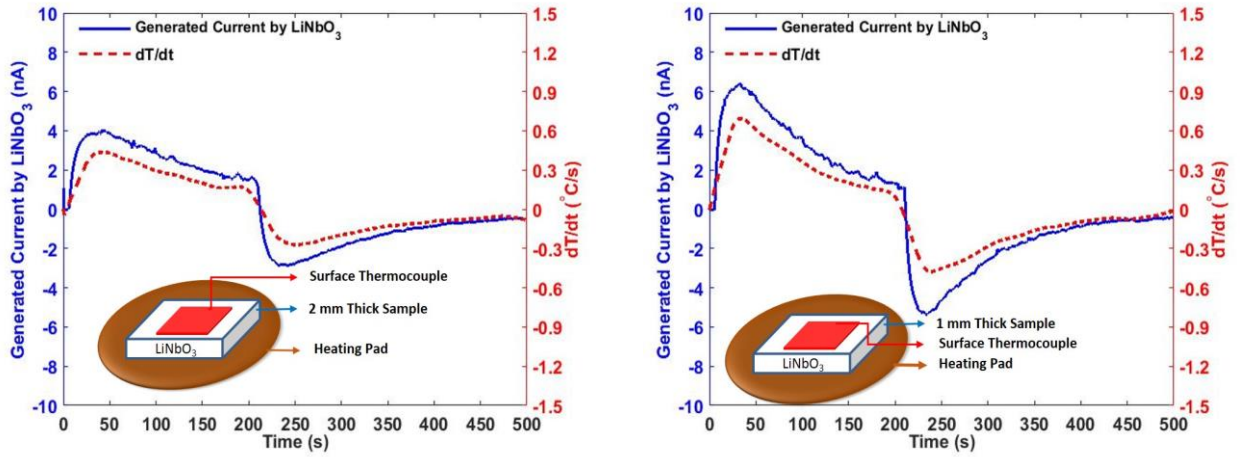

Figure 3.2: Generated current by $LiNbO_3$ and rate of temperature change of thermocouple mounted on top of 2 mm and 1 mm thick $LiNbO_3$

Both current profiles in Figure 3.2 matches with the rate of temperature change profile within experimental uncertainties satisfying Eq. (8). Figure 3.3 shows the current generation and corresponding temperature profile of thermocouple mounted on top of the 2 mm and 1 mm thick sample, respectively.

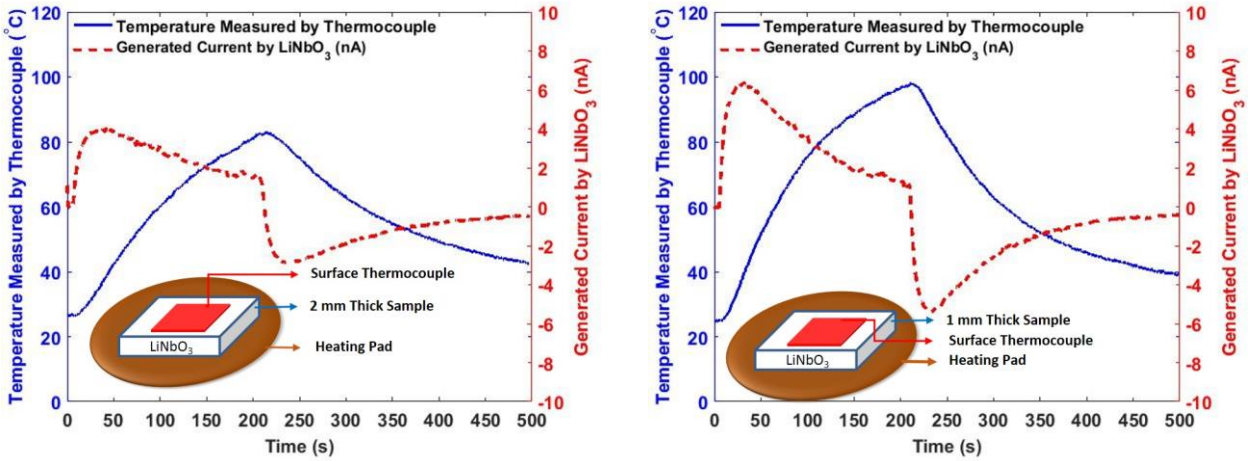

Figure 3.3: Generated current by $LiNbO_3$ and temperature profile of thermocouple mounted on top of the 2 mm and 1 mm thick $LiNbO_3$

Since $LiNbO_3$ could accurately measure the rate of temperature change, the feasibility of using $LiNbO_3$ instead of a thermocouple to sense temperatures in real time was then investigated.

The temperature of the sample at any time can be calculated from Eq. (10) and considering initial temperature as room temperature. All other parameters have explained in chapter 2 section 2.1.2 and 2.3. Figure 3.4 shows the results of measured temperature profiles by $LiNbO_3$ using their current output and applying that current in Eq. (10).

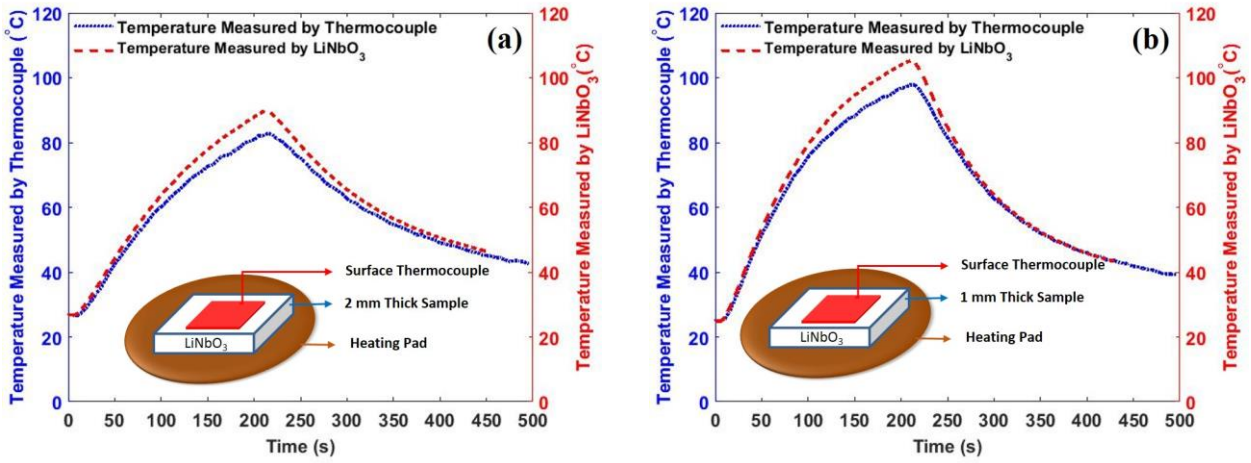

Figure 3.4: Temperature measured by thermocouple and a) 2 mm and b) 1 mm thick $LiNbO_3$

Figure 3.4 shows the comparison between temperatures measured by thermocouple and $LiNbO_3$. A maximum of 8 % and 6.7 % differences were found for the 2 mm and 1 mm thick sample, respectively. These differences were caused since the surface thermocouple was mounted on top of the sample. The temperatures measured by $LiNbO_3$ (dashed line in Figure 3.4) were calculated from the generated current due to the rate of temperature change experienced by their contact with the silicon heating pad. On the other hand, the thermocouple is mounted on top of the $LiNbO_3$ and both the thickness and silver paint act as a thermal barrier. Also the top surface of the $LiNbO_3$ and the thermocouple was open to the atmosphere, which causes a heat loss due to natural convection resulting in lower measurements by the surface thermocouple than the $LiNbO_3$ was actually experiencing. Therefore, in Figure 3.4, the differences between the temperatures measured by thermocouple and $LiNbO_3$ were observable where the dotted line represents the measurement by thermocouple and the dashed line represents the results from the

$LiNbO_3$ was actually experiencing. Here, the 2 mm thick $LiNbO_3$ has a higher difference than the 1 mm thick sample as the thickness acts as a dominating factor in the thermocouple readings.

To prove our hypothesis, two 1 mm thick $LiNbO_3$ sample sensors with the same dimensions (1 cm x 1 cm) were stacked together by placing a surface thermocouple between them to create a sandwich structure. In our hypothesis, the top sample will experience a lower temperature than the bottom sample due to thermal resistance. As shown in Figure 3.5, this sandwiched structure sample was placed on top of the silicon heating pad and an experiment was conducted by maintaining all other parameters constant with respect to previous tests, including heat flux, heating, and cooling time. Measured temperature by the thermocouple was compared with those measured by both the bottom and top $LiNbO_3$.

As shown in Figure 3.5, the result of temperature measured from the output current of the bottom $LiNbO_3$ (squared line) was higher than the measured temperature by the thermocouple (dashed line) as the thermocouple was measuring less temperature and the bottom sample was actually experiencing higher temperature. On the other hand, the temperature measured by the thermocouple was higher than the top $LiNbO_3$ was actually experiencing, resulting temperature measured by top $LiNbO_3$ (circled line) was lower than the temperature measured by thermocouple (dashed line). Also the bottom sample, thermocouple, and top sample reached their highest temperature after 213 s, 214 s and 219 s respectively, which implies the delay in measurement by the thermocouple and top sample. The result in Figure 3.5 explains the reason for the differences in Figure 3.4 between the temperature measurement by the thermocouple and $LiNbO_3$. It is possible to minimize the difference by minimizing the heat loss and also by using thinner $LiNbO_3$.

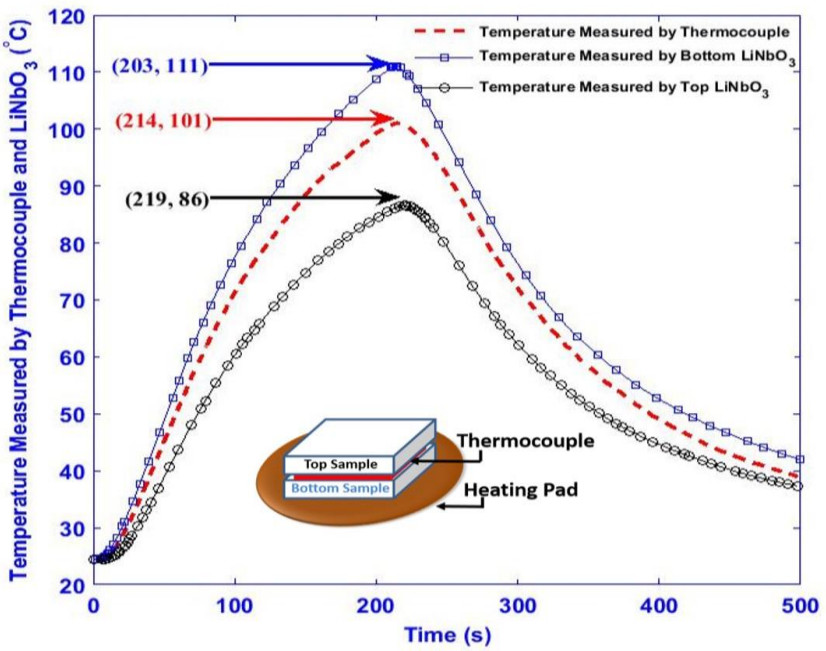

Figure 3.5: Temperature measured by the thermocouple and 1 mm thick sandwich structured $LiNbO_3$

Based on results presented for characterization of LNB with heating and cooling, it is feasible that $LiNbO_3$ ceramic materials could be used as a replacement sensor for low and high temperature applications. $LiNbO_3$ ceramic materials have several advantages over other invasive thermometry including thermocouples, resistive thermometry, and capacitive thermometry. For example, thermocouples require two homogeneous but dissimilar conductors requiring independent measurement of hot and cold junction temperature. The temperature sensor using $LiNbO_3$ is a single material and requires only room temperature as the reference point. Based on results presented here, the accuracy and response rate is comparable to those from a conventional thermocouple. Any differences in the two measurements were due to convective heat losses.

The next step of the project is to test LNB sample sensor for other operating conditions including low rate temperature change for a prolonged time and high rate of temperature change within a short time. The following sections shows the results for those operating conditions.

3.1.2 Temperature Measurement at Low Rate of Temperature Change with LNB

Experimental results are shown here to determine the temperature by LNB in low rate of temperature change environments with time. Figure 3.6 shows the low rate of temperature profile and current with respect to low rate temperature change with time. The solid line in Figure 3.6a is the temperature measured by the surface thermocouple on top of the $LiNbO_3$ with corresponding rate of temperature change with time. Figure 3.6b shows the generated current (solid line) by the $LiNbO_3$ sensor while on top of the silicon heating pad and experiencing low rate of temperature change with time (an average rate of .008 °C/s) until 650 s and remained at steady state condition for a prolonged time period within a small temperature range from 22.50 °C to 27.75 °C. In this specific condition, the generated current from the $LiNbO_3$ was used to calculate the temperature of the sensor using Eq. (10) and compared with the temperature measured by the thermocouple. Figure 3.7 shows the comparison between the temperature measured by the $LiNbO_3$ sensor (dotted line) and thermocouple (solid line) for a low rate of temperature change with time and a maximum 2 % of deviation was found between the two measurements at steady state condition.

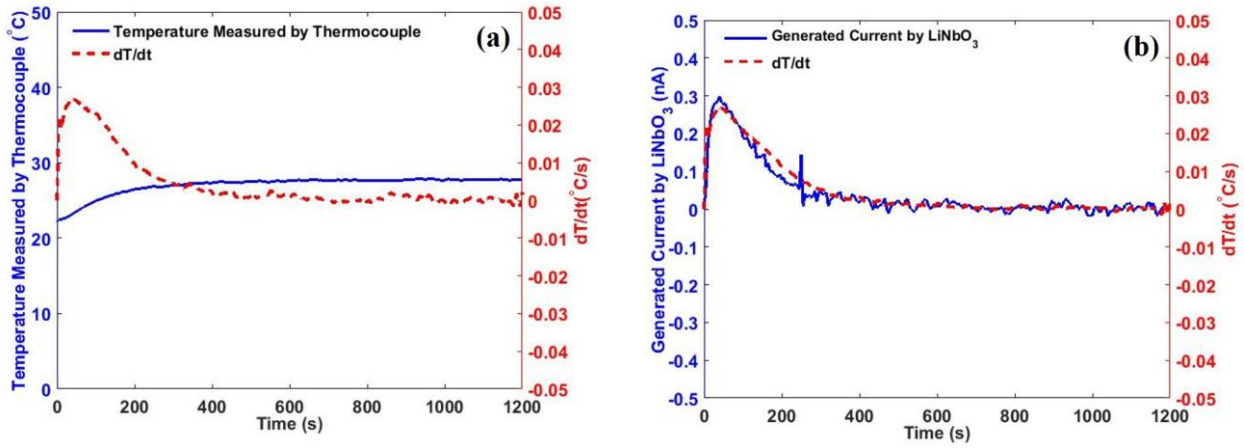

Figure 3.6: (a) Temperature profile with low rate of temperature change and b) Current profile with respect to low rate of temperature change with time

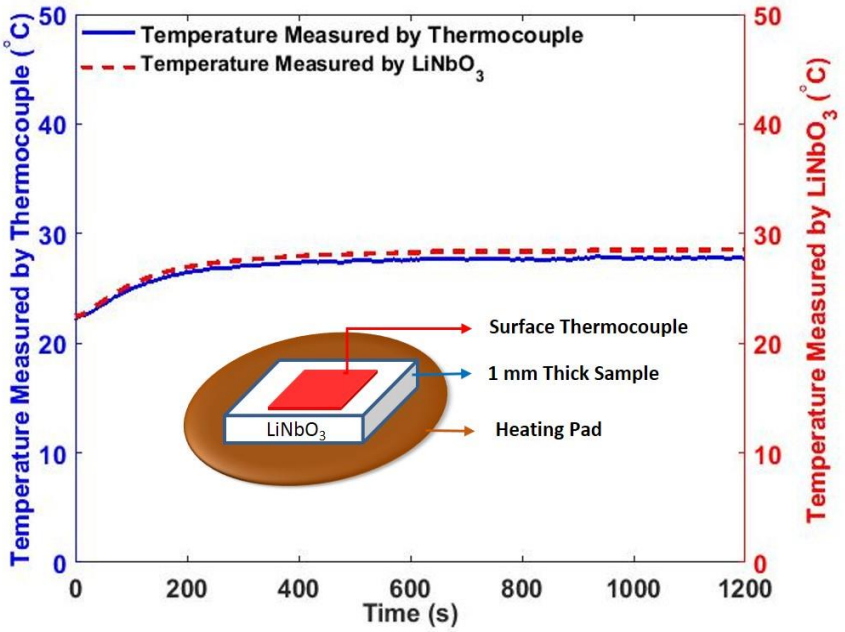

Figure 3.7: Temperature measured by the $LiNbO_3$ sensor and the thermocouple for a low rate of temperature change with time.

3.1.2 Temperature Measurement at High Rate of Temperature Change with LNB

Experimental results are shown here to determine the temperature by LNB in high rate of temperature change environment with time. Before the temperature measurements for a high rate of temperature change with time were done, an oven was set to 100 °C and maintained at a steady state condition for a prolonged time period. The LNB sensor along with a surface thermocouple attached on top of the sensor was then placed inside of the heated oven through a small opening. The surface thermocouple and the sensor were placed in the middle of the oven which was far from the oven's mounted thermocouple. Due to distance between the oven's thermocouple and surface thermocouple, the surface thermocouple was showing a lower temperature than the oven's reading. As the surface thermocouple was attached to the sensor, the temperature of the surface thermocouple was taken into consideration to compare with the temperature sensing reading from LNB sensor. Both sensor and thermocouple experienced high rate of temperature change (an average rate of 0.3 °C/s) until 190 s and remained at steady state

condition for a prolonged time period. Figure 3.8a shows the temperature profile with high rate of temperature change with time and Figure 3.8b shows the current profile with respect to high rate temperature change with time. In Figure 3.8b the difference between current profile and rate of temperature change profile is due to surface thermocouple has lower thermal load than LNB sensor. Due to this reason, the surface thermocouple response faster than the LNB sensor sample once they inserted inside of a pre-heated oven at the same time.

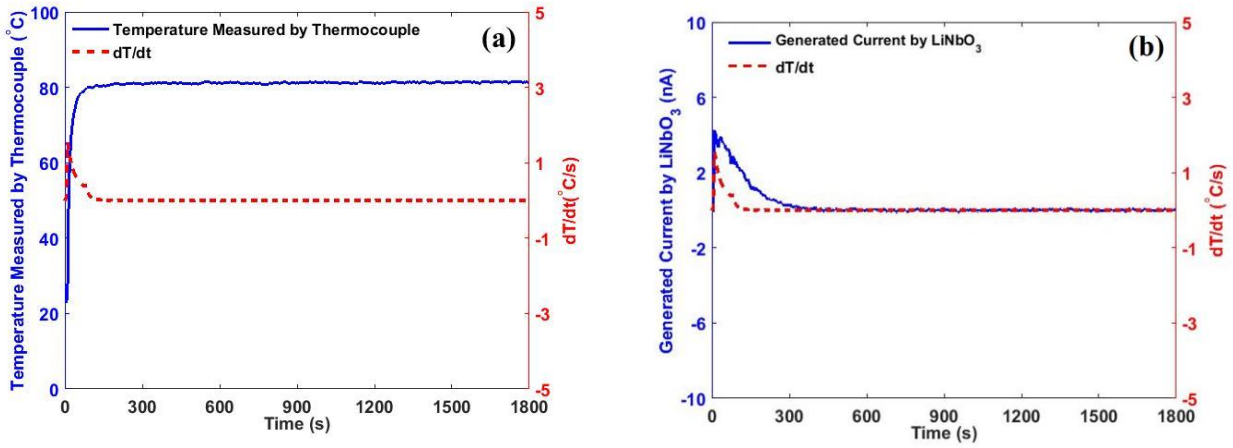

Figure 3.8: (a) Temperature profile with high rate of temperature change and b) Current profile with respect to high rate of temperature change with time

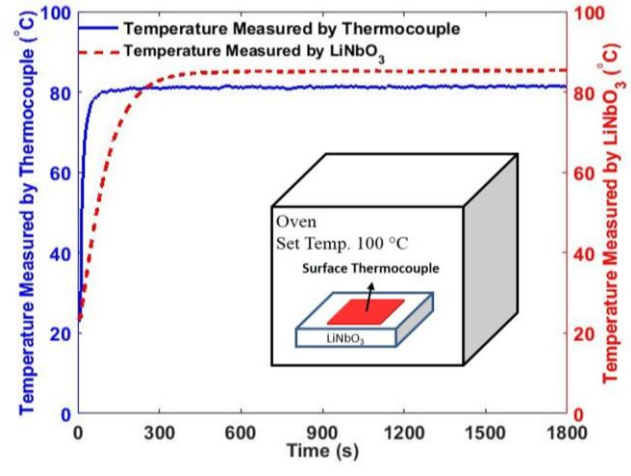

Figure 3.9: Temperature measured by the $LiNbO_3$ sensor and the thermocouple for a high rate of temperature change with time.

Figure 3.9 shows the comparison between the temperature measured by the $LiNbO_3$ (dotted line) sensor and the surface thermocouple (solid line) for oven test. Since the surface thermocouple has a lower thermal mass, hence lower response time compared to the $LiNbO_3$ sensor with dimensions of 1 cm x 1 cm x 0.2 cm. The surface thermocouple shows a sharp temperature change until it reaches a steady state condition. There is a maximum 4 % of deviation between the temperature measurement by the $LiNbO_3$ sensor and the thermocouple during steady state operating condition.

3.1.3 Pyroelectric Coefficient Measurement of LNB

This section shows the results of temperature dependent pyroelectric coefficient measurement using laboratory facilities for high temperature applications. In previous results sections, the sensor sample measured the temperature at low temperature range (<100 °C) by considering constant pyroelectric coefficient provided by the LNB manufacturer. For high temperature measurement, a temperature dependent pyroelectric coefficient is required. A dynamic pyroelectric coefficient measurement technique was applied to measure the pyroelectric coefficient. In this test, LNB sample sensor is subjected to experience cyclic heating and cooling with constant rate of temperature change with time. A sample sensor was prepared with high temperature resistive electrode and leads and placed inside of a tube furnace along with the rod thermocouple. Rod thermocouple was placed very close the sensor sample. This thermocouple measures the temperature is experiencing by the sensor sample. Figure 3.10 shows an example temperature profile applied to the sensor sample with its corresponding rate of temperature change with time.

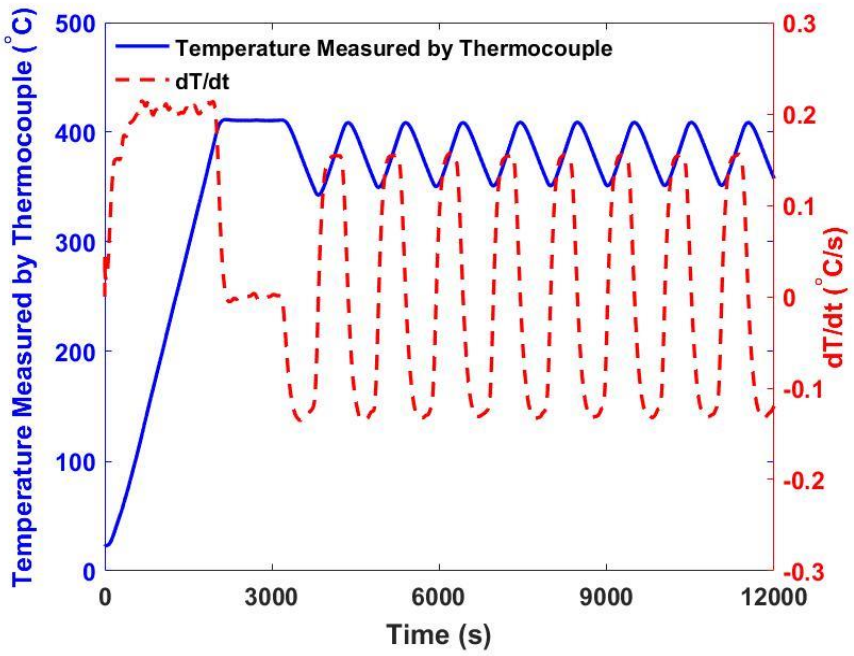

Figure 3.10: Temperature profile along with rate of temperature change with time using tube furnace on a LNB sample sensor

Based on the set temperature at tube furnace, the sensor experiences a temperature rise up to 410 °C within 35 minutes and remain constant for next 20 min. During these 20 min at constant 410 °C, the sample is experiencing zero rate of temperature change hence zero generation of current. Once the sample reaches at steady state conditions, a fluctuation of cyclic temperature was applied to the sample in between 410 °C to 350 °C with ±0.12 °C/s constant rate of temperature change. At the peaks of rate of temperature changes they reach ±0.12 °C/s constant rate of temperature change. At that moment, the generated current from the sample would be constant too. Figure 3.11 shows the generated current from the sample along with rate of temperature change.

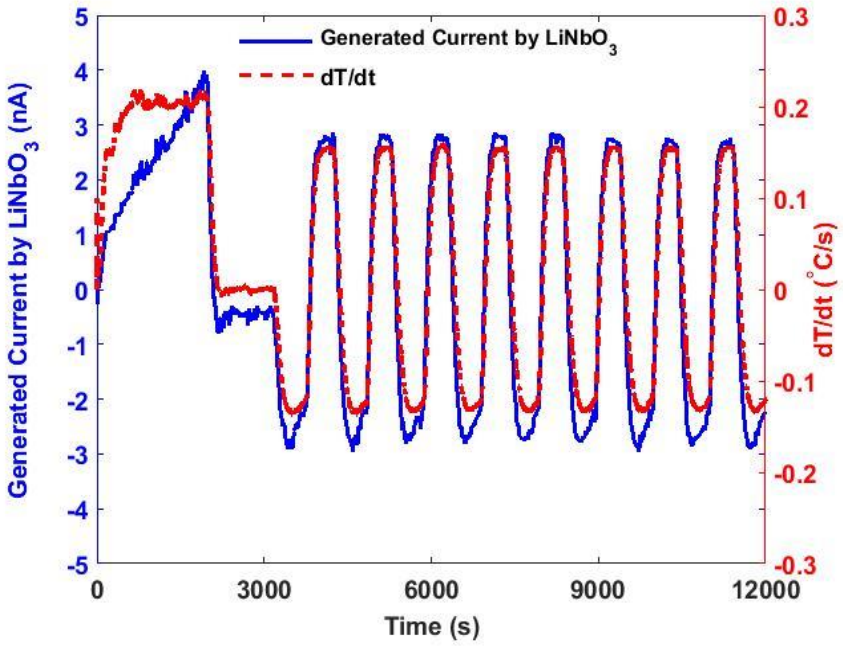

Figure 3.11: Generated current by LNB along with rate of temperature change with time

The current at the peaks were constant with constant rate of temperature change. This constant current value and the rate of temperature change were applied into Eq. (8) to calculate the pyroelectric coefficient for the range of 350 °C to 410 °C. Table 3.1 shows the temperature dependent pyroelectric coefficient of LNB with different temperature ranges.

Table 3.1: Measured temperature dependent pyroelectric coefficient of LNB using dynamic measurement technique

Temperature Range (°C)	Pyroelectric Coefficient, 10^{-5}, (C/m^2 °C)	Measurement Method
25-218	-8.5	Manufacturer Value
218-240	-14.85	Dynamic Test
257-292	-18.74	Dynamic Test
343-392	-21.81	Dynamic Test
350-410	-23.70	Dynamic Test
410-500	-23.70	Dynamic Test

3.1.4 Temperature Measurement at High Range (up to 500 °C) with LNB

For temperature measurements done at the high temperature range (up to 500 °C), the $LiNbO_3$ sensor was prepared using a high temperature resistive coating, adhesive and ceramic

sleeve (as shown in Figure 2.2). The $LiNbO_3$ sensor was then placed inside of a tube furnace, Figure 2.5, along with a thermocouple rod at room temperature condition with both ends of the tube open to the atmosphere. Later, the tube furnace was set at different operating conditions from room temperature to 500 °C respectively. At every operating condition, the thermocouple rod temperature readings were less than the set temperature of the furnace because the thermocouple rod was not at the same place as the furnace mounted thermocouple. As the thermocouple rod was placed close to the $LiNbO_3$ sensor, the temperature measured by the thermocouple rod was taken into consideration to compare with the temperature sensing reading from $LiNbO_3$ sensor. The current generated from $LiNbO_3$ sensor at different operating conditions was used to calculate the temperature of the sensor using Eq. (10). In Eq. (10) the temperature dependent pyroelectric coefficients were taken from Table 3.1.

Figure 3.12 to Figure 3.15 shows the comparison between temperature measured by the $LiNbO_3$ sensor (dotted line) and the thermocouple rod (solid line) at different set conditions of the tube furnace.

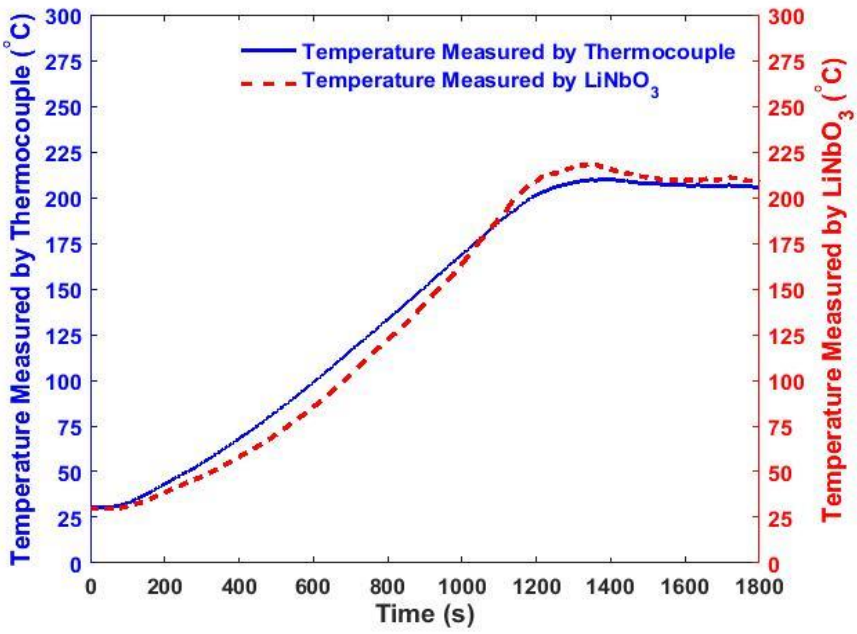

Figure 3.12: Temperature measured by the $LiNbO_3$ sensor and the thermocouple in a tube furnace up to 210 °C.

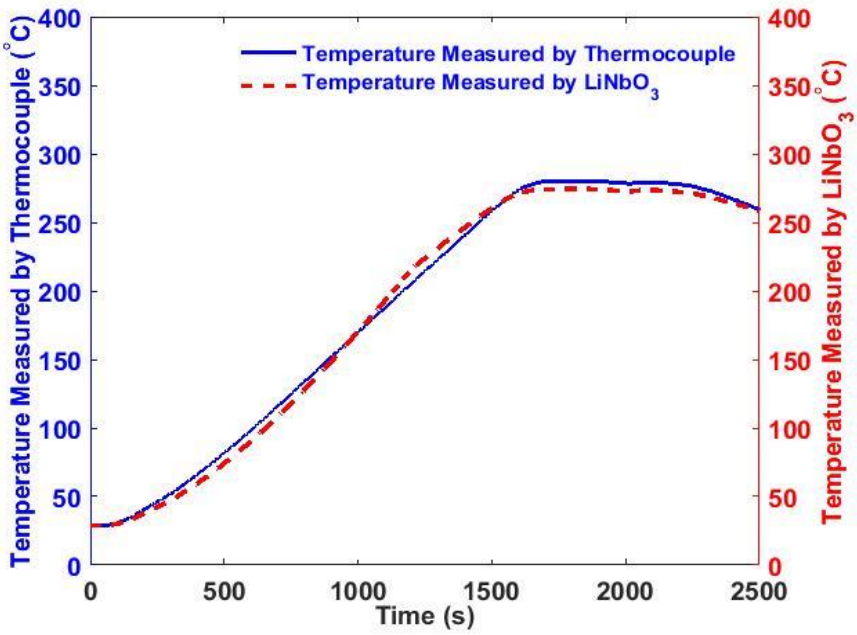

Figure 3.13: Temperature measured by the $LiNbO_3$ sensor and the thermocouple in a tube furnace up to 280 °C.

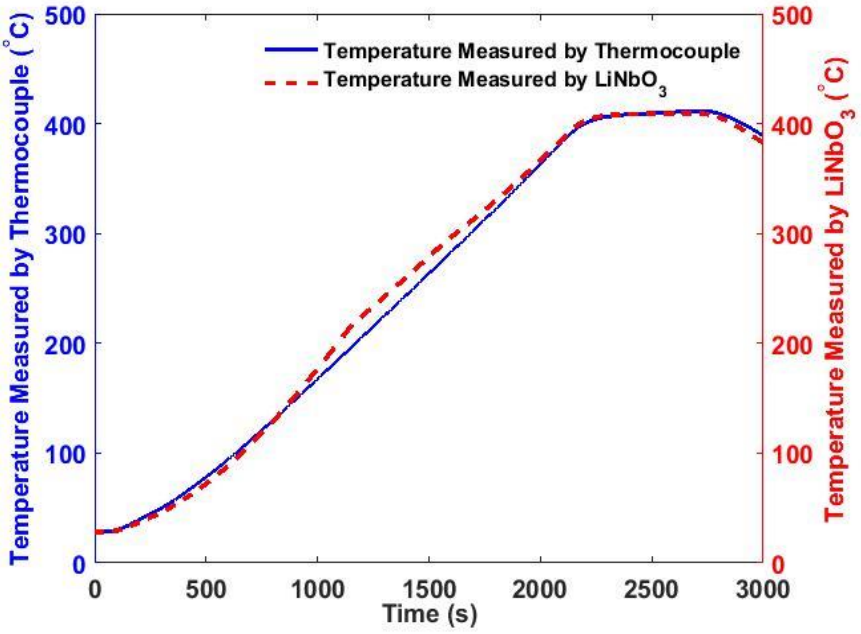

Figure 3.14 Temperature measured by the $LiNbO_3$ sensor and the thermocouple in a tube furnace up to 410 °C.

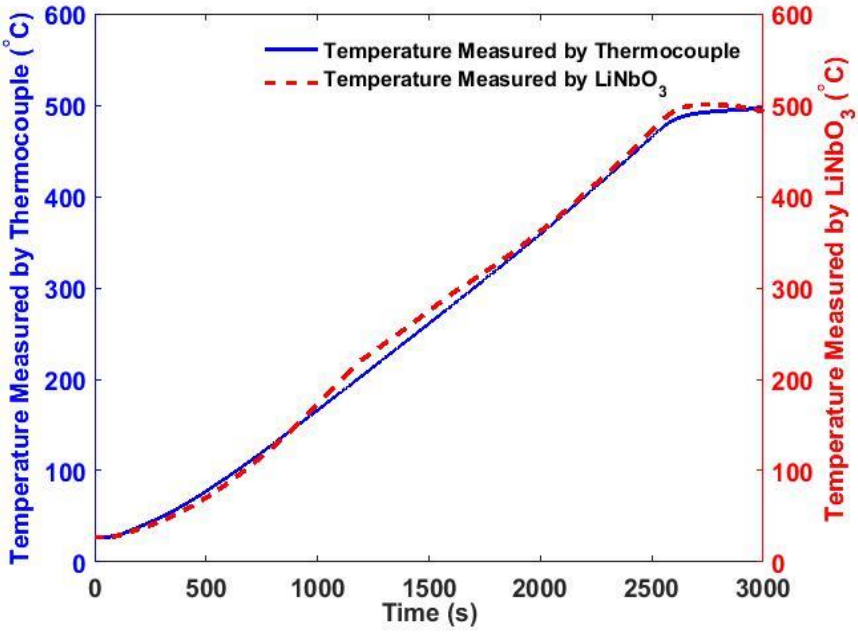

Figure 3.15: Temperature measured by the $LiNbO_3$ sensor and the thermocouple in a tube furnace up to 500 °C.

At every operating condition, the furnace temperature was maintained at a steady state condition for 600 s after it reached at highest set temperature for steady state sensing characterization. At the first operating condition, Figure 3.12, the thermocouple and the sensor measured the maximum temperature of 209 °C and 218 °C, respectively while at steady state condition. A 4.31 % deviation was determined between these points during while at a steady state condition. For the second, third, and fourth operating conditions, (Figure 3.13, Figure 3.14, and Figure 3.15 respectively) the measurements between the thermocouple and the sensor deviated by 2.1 %, 0.4 % and 0.6 % respectively at steady state condition. Since the two ends of the tube furnace were open to the atmosphere, convective heat transfer losses due to high temperature gradient impacted the magnitude of measurements between the thermocouple and sensor.

Overall, the study of temperature measurement at different operating condition with $LiNbO_3$ shows a methodology for measuring temperature using the pyroelectric properties of a $LiNbO_3$ ceramic material. Hence, it is possible to measure high temperatures using $LiNbO_3$,

providing the temperature dependent pyroelectric coefficient profile with respect to temperature is known.

3.2 Second Phase Experimental Results

This section shows the results for the characterization of magnetic field measurement using a Gaussmeter at different position of the electromagnet including at the center, at the edge, and at different distances apart from the edge of the electromagnet. Later, the gaussmeter output were used to measure the temperature of the PZT sensor wirelessly.

3.2.1 Characterization of Magnetic Field Measurement using a Gaussmeter

The gaussmeter probe was placed at different positions of the electromagnet including at the center of the electromagnet, at the edge, at 1.27 cm apart from the edge and 1.54 cm apart from the edge of the electromagnet. PZT sample sensor was placed on top of a hot plate and the temperature was set up to 110 °C and then cooled down naturally. A surface thermocouple was placed on top of the sample to get the PZT temperature. Figure 3.16 shows the PZT sample temperature and rate of temperature change with time for all the tests to characterize the magnetic field measurement using gaussmeter.

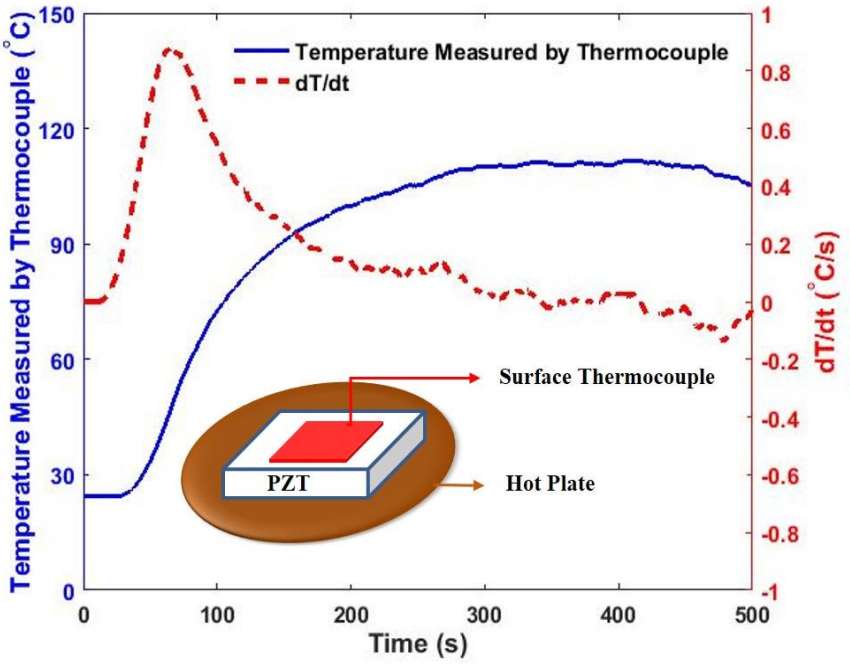

Figure 3.16: Temperature and rate of temperature change with time for PZT on top of a hot plate

Two leads from top and bottom surfaces of the PZT were connected with a picoammeter and an electromagnet in series connection. Generated current due to rate of temperature change with time experienced by PZT was measured by the picoammeter and the generated magnetic field due to passing the same current through the electromagnet was measured by gaussmeter. The following Figure 3.17 to 3.20 show the generated current due to experiencing rate of temperature change with time and the wireless readability of the magnetic field by the gaussmeter at different distances from the electromagnet including at the center of the electromagnet (Figure 3.17), at the edge of the electromagnet (Figure 3.18), at 1.27 cm apart from the edge of the electromagnet (Figure 3.19), and 1.54 cm apart from the edge of the electromagnet (Figure 3.20).

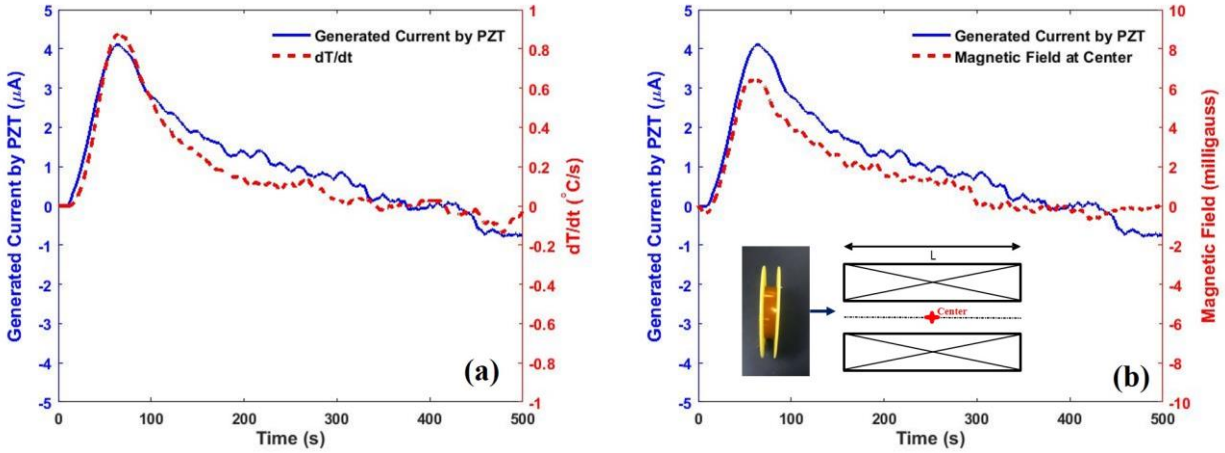

Figure 3.17: a) Current from PZT due to experiencing rate of temperature change with time (dT/dt) b) Magnetic field at the center due to current passing through the electromagnet

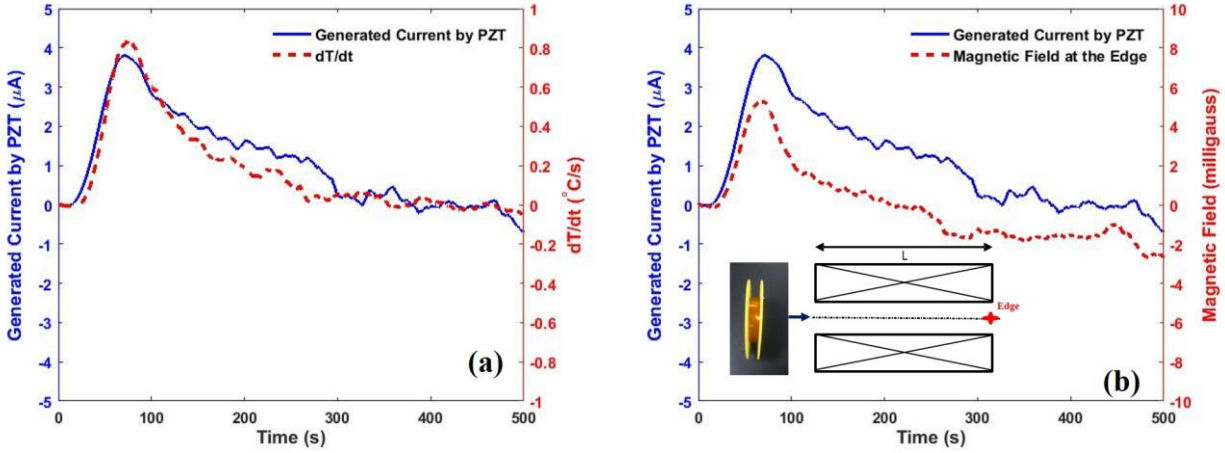

Figure 3.18: a) Current from PZT due to experiencing rate of temperature change with time (dT/dt) b) Magnetic field at the edge due to current passing through the electromagnet

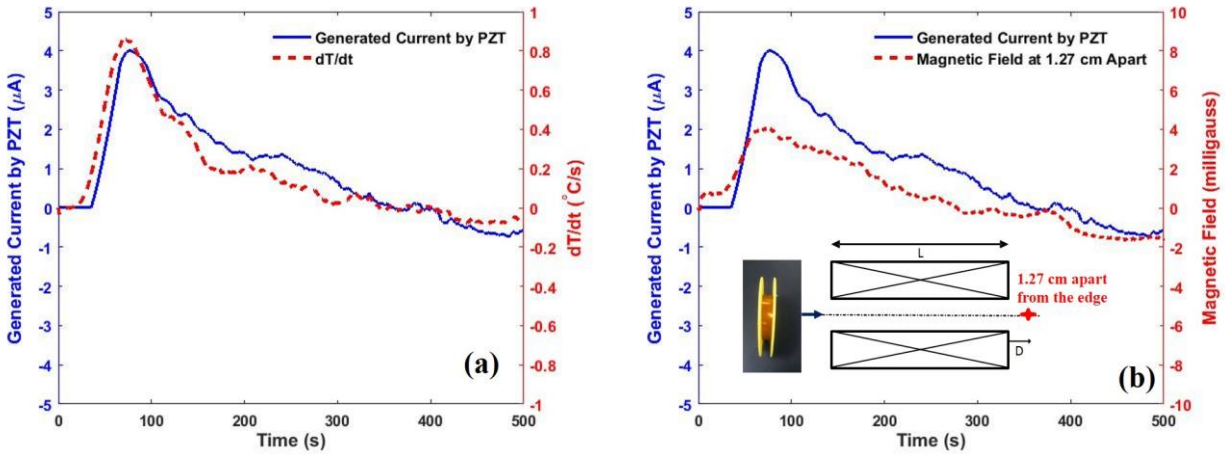

Figure 3.19: a) Current from PZT due to experiencing rate of temperature change with time (dT/dt) b) Magnetic field at 1.27 apart from the edge due to current passing through the electromagnet

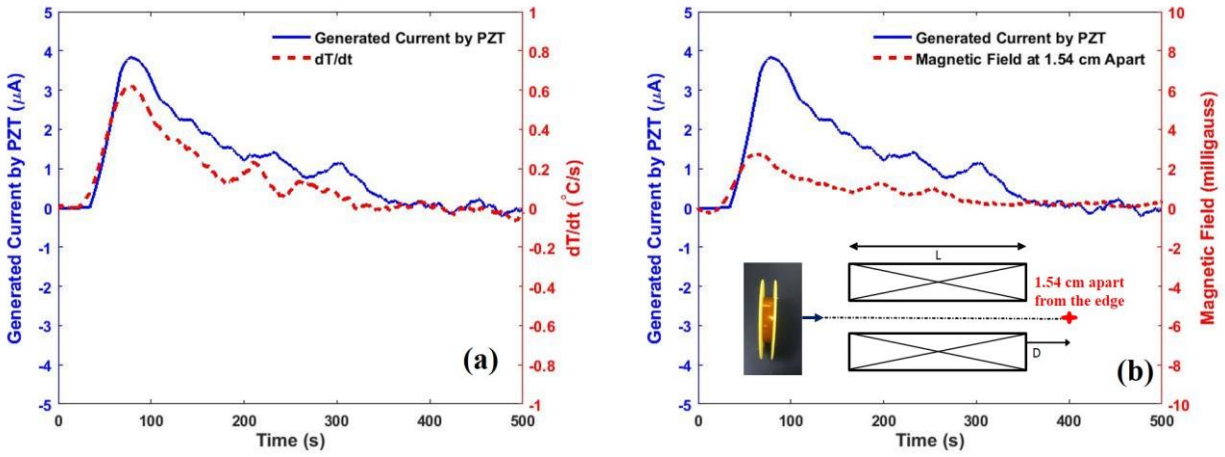

Figure 3.20: a) Current from PZT due to experiencing rate of temperature change with time (dT/dt) b) Magnetic field at 1.54 apart from the edge due to current passing through the electromagnet

From Figure 3.17 to 3.20, it was found that the magnetic field went down with increasing distances from the center of the electromagnet along its axis. Current profiles and magnetic field profiles in Figure 3.17 to 3.20 also followed the same trend thus satisfying the Eq. (14). Table 3.2 shows the comparison between analytical magnetic field and experimental magnetic field for the maximum amount of current supplied to the electromagnet.

Table 3.2: Analytical and experimental magnetic field for the maximum current passing through the electromagnet at different positions

DC Milligaussmeter Probe Position	Peak Current Supplied to the Electromagnet from PZT (μA)	Analytical Magnetic Field (milligauss)	Experimental Magnetic Field (milligauss)	Deviation (%)
At the center of the electromagnet	4.59	7.22	8.06	11
At the edge of the electromagnet	4.27	6.22	6.2	0.4
At 1.27 cm apart from the edge of the electromagnet	4.50	5.82	4.55	11
At 1.54 cm apart from the edge of the electromagnet	4.34	3.33	3.30	0.9

All the physical parameters of the electromagnet including length, inner and outer radius were measured with ruler scale, slide calipers, and micrometer. Different positions of the gaussmeter probe from the edge of the electromagnet were also measured with ruler scale. Small changes in the dimensions of the physical parameter causes significant changes of analytical and experimental magnetic field. The deviations between analytical and experimental magnetic field were due to the uncertainty of the physical parameters of the electromagnet and the gaussmeter probe distances from the edge of the electromagnet. Figure 3.21 (a) to (d) show the graphical comparison between analytical and experimental magnetic field measured at different positions from the edge of the electromagnet. Figure 3.22 only shows the experimental magnetic field at different positions of the electromagnet.

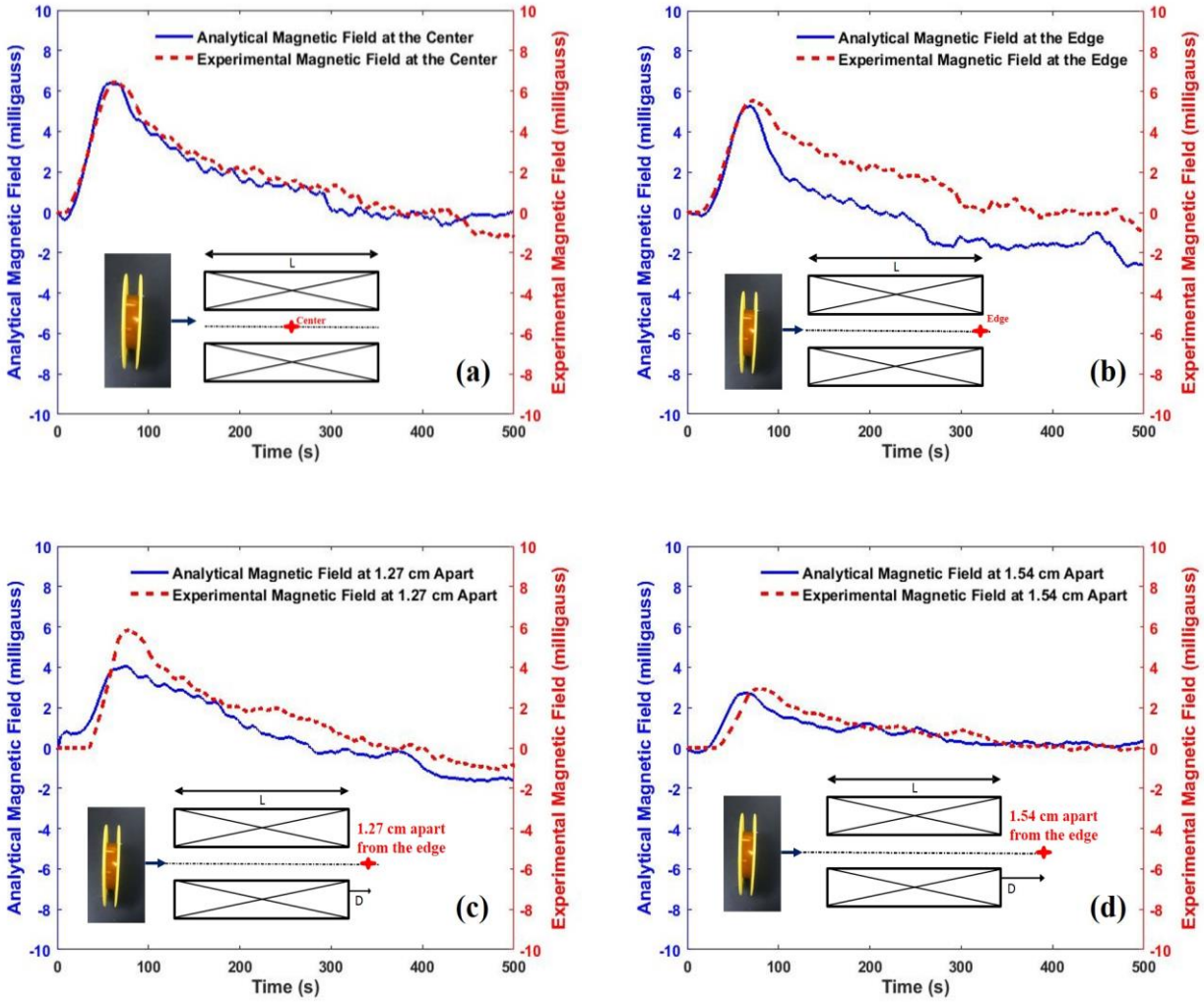

Figure 3.21: Graphical comparison of analytical and experimental magnetic field at different positions of the electromagnet: a) at the center, b) at edge, c) at 1.27 cm apart from the edge, and d) at 1.54 cm apart from the edge

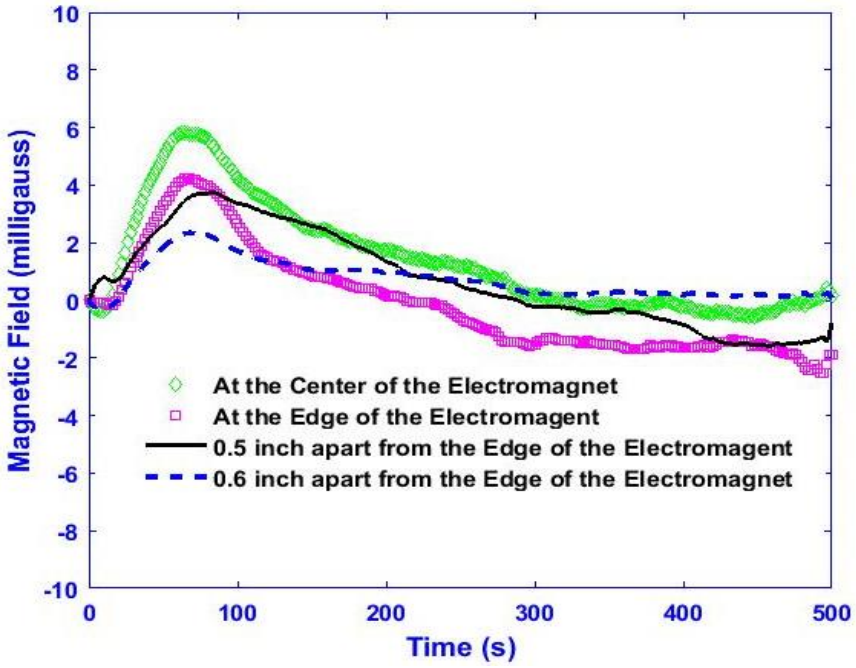

Figure 3.22: Comparison of magnetic field measured at different position of the electromagnet

As the magnetic field decreases with the increasing of distance from the edge of the electromagnet along its axis, a nickel/iron/molybdenum alloy core material was placed at the center of the electromagnet. The purpose of inserting a core material at the center of the electromagnet was to increase the magnetic field strength by a factor of magnetic permeability of the core material. Figure 3.23 shows the experimental magnetic field measurement by placing the gaussmeter probe at 1.54 cm apart from the edge of the electromagnet with and without core material.

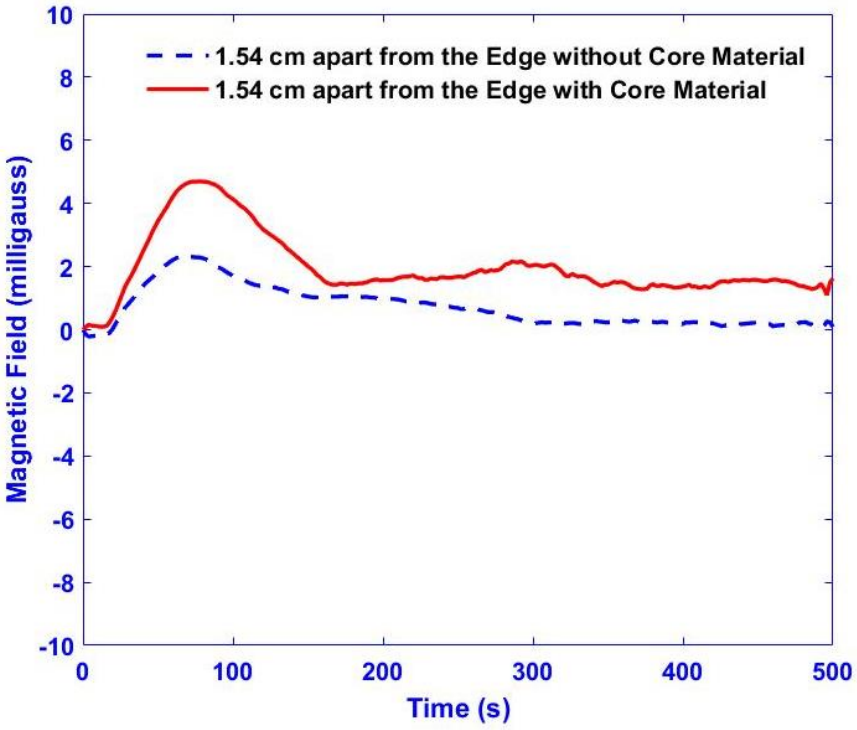

Figure 3.23: Measured magnetic field at 1.54 cm apart from the edge of the electromagnet with and without core material

From Figure 3.23, it was found that at maximum current supply from the PZT to the electromagnet, the magnetic field was increased twice with core material than without core material. In Figure 3.16 and 3.23, the PZT sample started reaching steady state condition in between 200 s to 500 s. In this time period the rate of temperature change was constant and reached near zero and there was near zero generation of current also. Theoretically in this time frame (between 200 s to 500 s), magnetic field profile should follow the rate of temperature change with time (dT/dt) profile (Figure 3.16). The magnetic field without core material has the same trend with the rate of temperature change with time (Figure 3.16). On the other hand, when the electromagnet had a core material inside the gaussmeter measured significant higher magnetic field than without core material in the time frame between 200 s to 500 s. This phenomenon indicated about the induced magnetic field on the core material after applying current from the PZT to the electromagnet. Due to this induced magnetic field, the gaussmeter was measuring magnetic field even the PZT sample was not experiencing any rate of

temperature change. As the final approach of this project was to use the measured magnetic field by gaussmeter to calculate the temperature experienced by the PZT, the induced magnetic field on the core material was not allowable. To use the PZT sample as a sensor material to measure the temperature wirelessly, electromagnet without core material was used. The next section of the results show the wireless temperature measurement using PZT ceramic material.

3.2.2 Wireless Temperature Measurement

The PZT sample was subjected to test in two different set temperatures by the hot plate. For the first test, the hot plate was set to reach up to 100 °C and then let it cooled naturally. Figure 3.24 (a) and (b) shows the generated current by the PZT and the corresponding theoretical magnetic field (calculated from current measured by picoammeter using Eq. (13) and experimental magnetic field (measured by gaussmeter at 0.254 cm apart from the edge of the electromagnet) respectively for 100 °C set temperature of the hot plate.

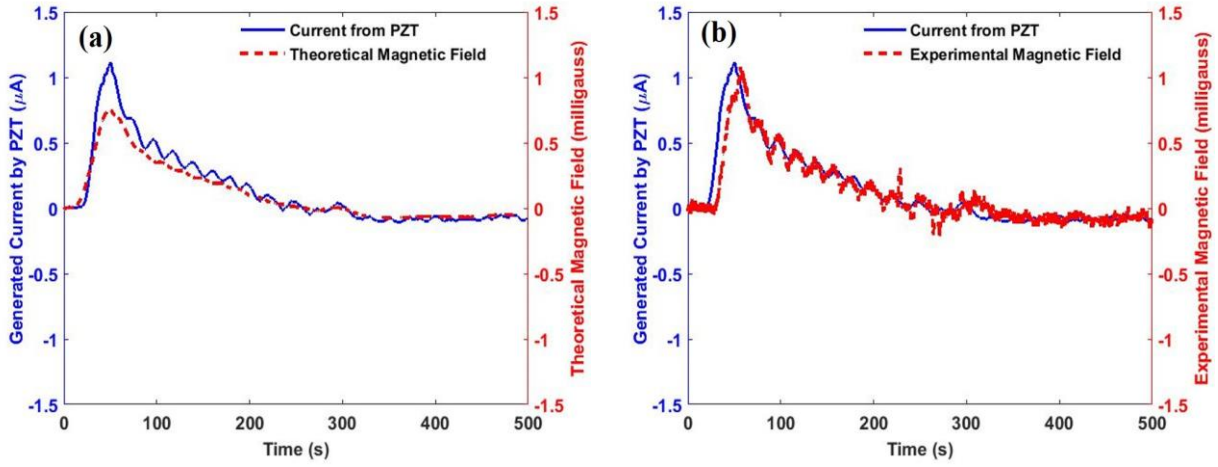

Figure 3.24: Generated current by PZT with corresponding a) Theoretical magnetic field and b) Experimental magnetic field (Hot plate set temp. 100 °C)

A comparison of theoretical and experimental magnetic field has shown in Figure 3.25 where both have the same profile. Calculated temperature from these two magnetic field using Eq. (16) should match each other.

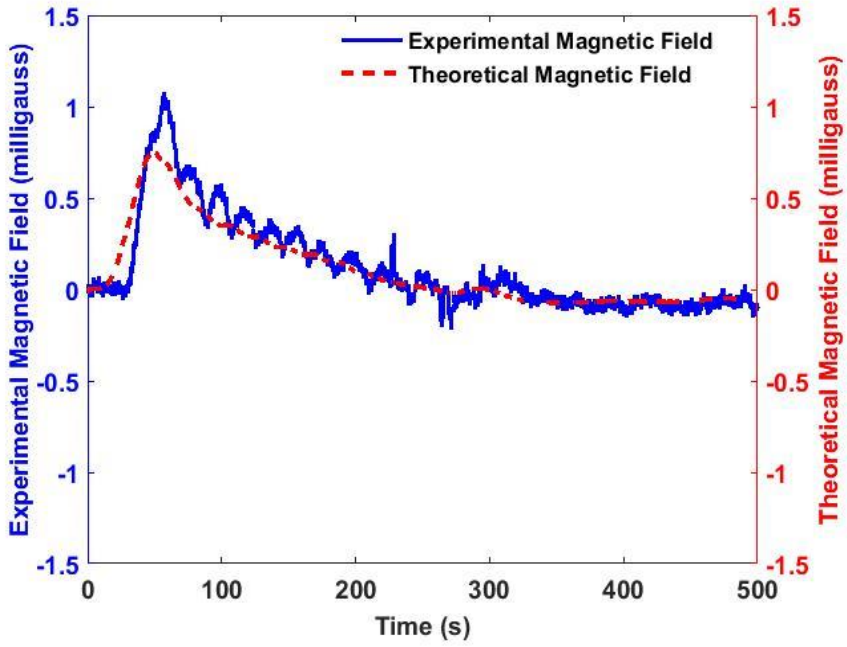

Figure 3.25: Experimental and theoretical magnetic field for PZT at 100 °C set temperature

Figure 3.26 shows the comparison between thermocouple temperature and the temperature measured by using theoretical and experimental magnetic field in Eq. (16). The surface thermocouple temperature (dotted line) is higher than the temperature measured from theoretical magnetic field (dashed line) and experimental magnetic field (straight line). As the surface thermocouple had the point contact compare to the large surface area of the PZT sample, it was not measuring the actual overall surface temperature of the sample.

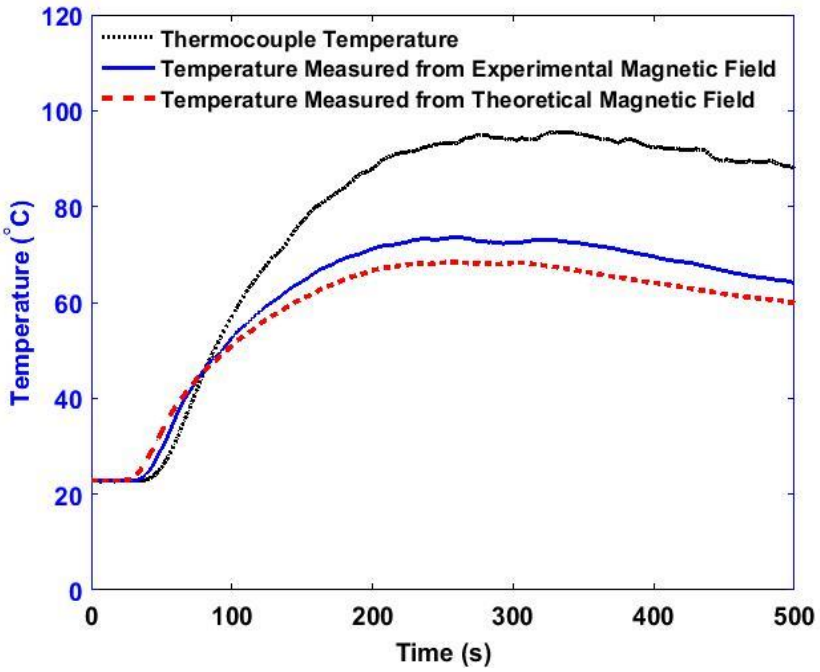

Figure 3.26: Comparison between thermocouple temperature and temperature measured by theoretical and experimental magnetic field (Hot plate set temp. 100 °C)

A thermal imaging technique was also performed to see the overall surface temperature of the sample. Figure 3.27 shows the thermal images of the sample taken with an IR camera during the experiment. From Figure 3.27 (a), it was found that the sample temperature was evenly distributed before starting the test. From Figure 3.27 (b) it was found that the sample temperature was not evenly distributed after certain time once the test started.

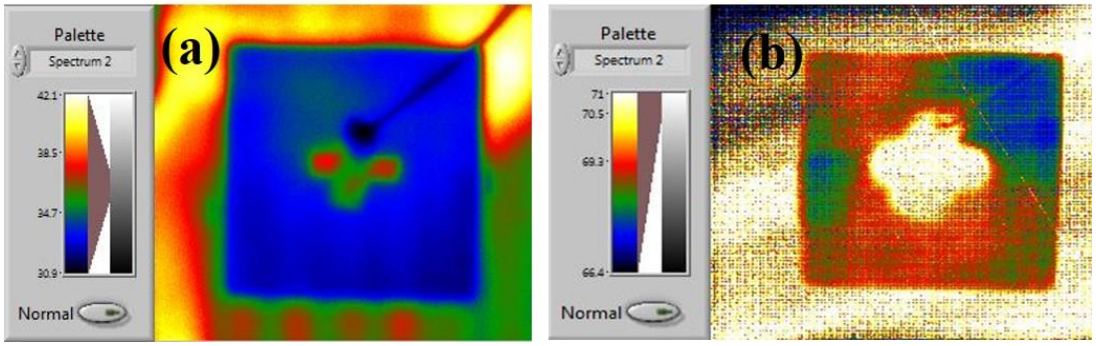

Figure 3.27: Thermal Image of the PZT sample during two different operating conditions a) Before starting the test b) During the test after certain time

This uneven distribution of the sample temperature proved the difference between the thermocouple temperature and the temperature measured by the theoretical magnetic field and experimental magnetic field. The pyroelectric current generation from the PZT sample was from the overall rate of temperature change it was actually experiencing, not from the rate of temperature change measured by the surface thermocouple with a point contact. Due to this reason, the calculated temperature from experimental magnetic field was compared with temperature measured with theoretical magnetic field and maximum 7.5% deviation was found.

The PZT sample sensor was also subjected to test at different temperature by setting the hot plate temperature up to 120 °C. Figure 3.28 (a) and (b) shows the generated current by the PZT and the corresponding theoretical magnetic field (calculated from current measured by picoammeter using Eq. (13)) and experimental magnetic field (measured by gaussmeter at 0.254 cm apart from the edge of the electromagnet) respectively for 120 °C set temperature of the hot plate. A comparison of theoretical and experimental magnetic field has shown in Figure 3.29 where both have the same profile. Figure 3.30 shows the comparison between thermocouple temperature and temperature measured from theoretical and experimental magnetic field.

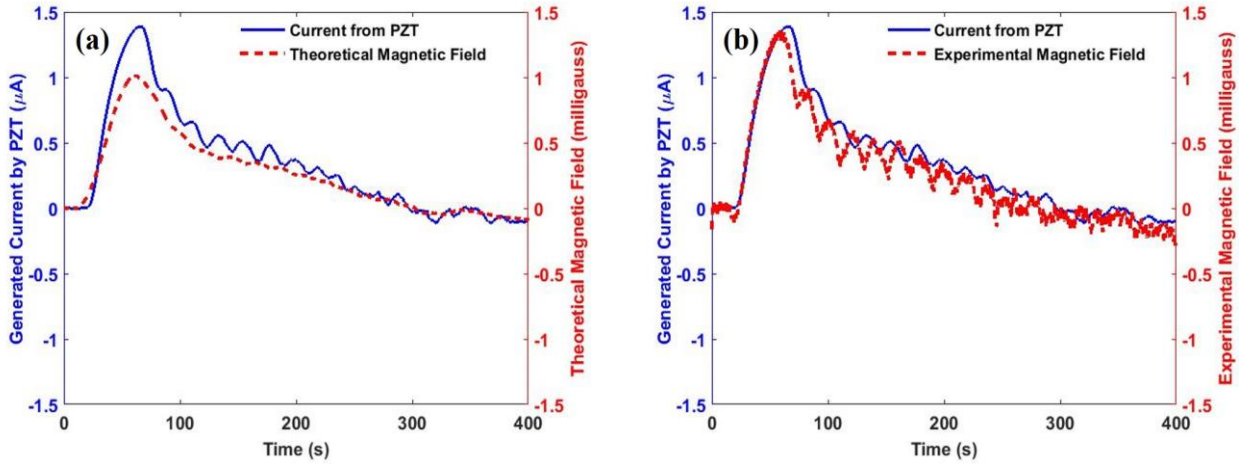

Figure 3.28: Generated current by PZT with corresponding a) Theoretical magnetic field and b) Experimental magnetic field (Hot plate set temp. 120 °C)

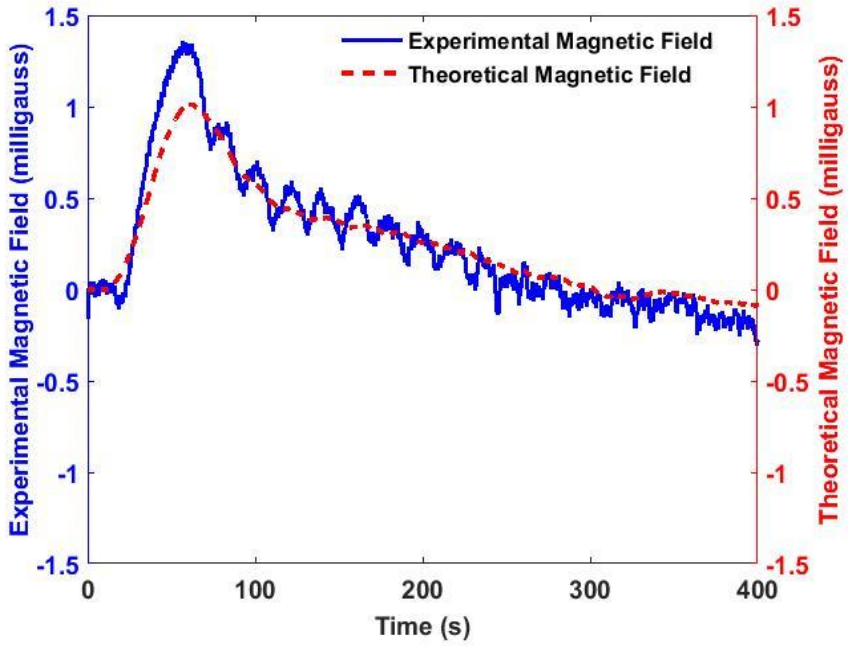

Figure 3.29: Experimental and theoretical magnetic field for PZT at 120 °C set temperature

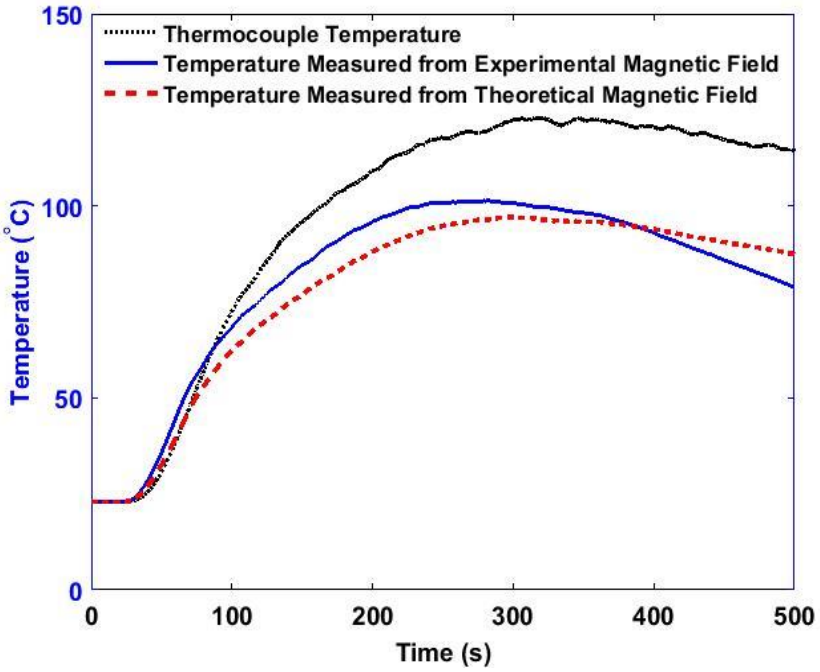

Figure 3.30: Comparison between thermocouple temperature and temperature measured by theoretical and experimental magnetic field (Hot plate set temp. 120 °C)

For the second test at 120 °C, the temperature measured from experimental magnetic field was also compared with the temperature measured from theoretical magnetic field and

similar profile characteristics were found as the first at 100 °C. A maximum 4.3 % deviation was found between the temperature measured from theoretical and experimental magnetic field. For both tests (set temp. 100 °C and 120 °C), multiple experiments were performed and deviations were found within 7.5 %. These deviations may come from the physical parameters of the electromagnet those were used in Eq. (13) including number of turns, length of the electromagnet, inner radius, and outer radius.

This study shows the feasibility and readability of measuring temperature using PZT ceramic material wirelessly up to 100 °C by considering constant pyroelectric coefficient provided the PZT manufacturer at room temperature conditions. Hence, it is possible the measure the temperature wirelessly with pyroelectric ceramic material up to their Curie temperature by knowing the temperature dependent pyroelectric coefficient.

CHAPTER 4 CONCLUSIONS AND FUTURE WORKS

4.1 Conclusions

4.1.1 High Temperature Measurement with LNB

A temperature measurement methodology was developed using pyroelectric properties of ceramic materials with wired connections and with a wireless connection. Single crystal pyroelectric ceramic materials were purchased commercially and used as sensor materials. Pyroelectric materials generate current while experiencing rate of temperature change with time. The generated current was taken into consideration to calculate the temperature.

Lithium niobate, LNB ($LiNbO_3$) ceramic material was used to develop the temperature sensor with wired connection. Different operating conditions were applied to the LNB sample sensor including cyclic heating and cooling, low rate of temperature change, high rate of temperature change at low temperature ranges (<100 °C). At this temperature range, the pyroelectric coefficient value of LNB was considered (-8.5×10^{-5} C/m^2 °C)

For cyclic heating and cooling 8 % and 6.7 % deviation were found for 2 mm and 1 mm thick sample. A sandwich structured LNB samples of 1 mm thick sample was developed and tested for cyclic heating and cooling and it was found that the deviation goes down with thinner sample.

For the low and high rate of temperature change conditions, the LNB sensor measure the temperature with 2% and 4% deviation respectively. LNB sensor temperature was compared with the temperature measured by the surface thermocouple at the same time. For high rate of temperature change with time, the deviation increased as the sample sensor has higher thermal load compare to surface thermocouple.

The LNB sensor was also tested for high temperature measurements. Before high temperature measurement testing, the temperature dependent pyroelectric coefficient of LNB was measured with dynamic pyroelectric coefficient measurement technique for different temperature ranges up to 500 °C. Temperature dependent pyroelectric coefficient of LNB was

found in between -8.5 x 10^{-5} C/m^2 °C to -23.7 x 10^{-5} C/m^2 °C from room temperature to 500 °C. This temperature dependent pyroelectric coefficient values were used to calculate the temperature using LNB for high temperature measurement up to 500 °C. The LNB sample sensor was placed inside of a tube furnace and different temperatures were set at the tube furnace. For different set temperatures of the tube furnace, the LNB sensor measures the temperature up to 220 °C, 280 °C, 410 °C and 500 °C with 4.31 %, 2.1 %, 0.4 % and 0.6% deviation, respectively. Overall, the LNB sensor with wire connection was able to measure the temperature at different operating conditions up to 500 °C with maximum 8 % deviation.

4.1.2 Wireless Temperature Measurement with PZT

For developing wireless temperature sensor, PZT ceramic material was used to measure the temperature for its higher signal strength with higher pyroelectric coefficient compare to LNB. An electromagnet was built using university facilities with a pre-designed number of loops of wire, length, inner radius and outer radius. The PZT was connected with a picoammeter and an electromagnet in series connection. Picoammeter measured the current passing through the electromagnet and a gaussmeter measured the magnetic field generated from the electromagnet.

At first the electromagnet was characterized by detecting the magnetic field with a gaussmeter from various distances of the electromagnet including at the center, at the edge, at 1.27 cm, and 1.54 cm apart from the edge of the electromagnet along its axis. The PZT sample was supplying maximum 4.59 µA current with corresponding maximum 0.84 °C/s rate of temperature change with time, and the current was supplied to the electromagnet to generate magnetic field. The gaussmeter was able to detect the magnetic field at the center, at the edge, at 1.24 cm, and 1.54 cm apart from the edge of the electromagnet with 11 %, 0.4 %, 11 %, and 0.9 % deviation, respectively. A nickel/iron/molybdenum alloy core material was also placed inside of the electromagnet to intensify the magnetic field strength by the factor of magnetic permeability of the core material. Gaussmeter measured the magnetic field 1.54 cm apart from the edge of the electromagnet along its axis with and without core material inside of the

electromagnet. The electromagnet with core material intensified the magnetic field by a factor of two then the electromagnet without the core material. It was also found that the core material was experiencing induced magnetic field after removing current flow through the electromagnet. As the magnetic field was used to calculate the temperature of the PZT, the induced magnetic field on the core material was not desirable. Due to this, the PZT sample and electromagnet without core material were prepared to measure the temperature wirelessly.

Two different temperature (100 °C and 120 °C) was applied to the PZT ceramic material by placing it on top of a hot plate. The generated current was measure by picoammeter and the generated magnetic field from the electromagnet was measured with a gaussmeter probe at 0.254 cm apart from the edge of the electromagnet.

PZT temperature was calculated from both theoretical and experimental magnetic field and compared. PZT temperature was not compared with the surface thermocouple temperature. Surface thermocouple has a small point contact compare to PZT surface area and cannot measure the overall temperature of the PZT. During the testing, PZT was experiencing uneven distribution of temperature which was seen by taking images with an IR camera. The generated current from PZT was from that uneven temperature distribution. Due to this reason, the calculated temperature of PZT from experimentally measured magnetic field was compared with the theoretical magnetic field. For two operating conditions (100 °C and 120 °C), the PZT sample was able to measure the temperature wirelessly with maximum 7.5 % and 4.3 % deviation from the theoretical current respectively.

4.2 Future Works

For current study, we were able to use lithium niobate (LNB) ceramic material as a sensor to measure the temperature up to 500 °C. Temperature dependent pyroelectric coefficients were experimentally measured up to 500 °C and used for sensing temperature. In literature, temperature dependent pyroelectric coefficients were found up to 450 °C for LNB. But, LNB has

a Curie temperature 1210 °C and it is possible to use it as a temperature sensor up to its Curie temperature. Due to lacking of available resources of temperature dependent pyroelectric coefficient values for LNB, we will follow three different methods to measure the temperature dependent pyroelectric coefficients up to 1210 °C including static, indirect, and dynamic measurement technique. The best result, from these three different pyroelectric coefficient measurement techniques will be used for the LNB sensor to measure the temperature up to 1210 °C. System development (section 2.3) for temperature measurement will be improved by packaging the sensing system. The sensor package will then be tested in real field environment.

We have also used LNB for waste heat energy harvesting by applying heating and cooling rate of temperature change with time to the LNB using thermoelectric cooler for low temperature range (up to 60 °C) [23]. For low temperature range, the pyroelectric coefficient was -8.5×10^{-5} C/m^2 °C. From our investigation while measuring temperature dependent pyroelectric coefficient with dynamic technique, it was found that the pyroelectric coefficients were higher in high temperature ranges (Table 3.1). These findings imply that LNB will store higher energy for same rate of temperature change with time for high temperature ranges then the low temperature ranges. Most of the energy harvesting methods and electronic components are for low temperature ranges and very few have been found for high temperature and extreme negative temperature applications. Our next effort would be for energy harvesting from extreme temperature conditions like gas turbine, jet engine, oxy-fuel combustion, gas-solid fluidized beds, and from outer spaces in satellites. We have also used PZT ceramic material for wireless temperature measurement which can also be used for wireless energy harvesting by using magnetic field.

REFERENCES

[1] Riza, Nabeel A., and Mumtaz Sheikh. "All-silicon carbide hybrid wireless-wired optics temperature sensor network basic design engineering for power plant gas turbines." *International Journal of Optomechatronics* 4, no. 1 (2010): 83-91.

[2] Wang, Ya, Yi Jia, Qiushui Chen, and Yanyun Wang. "A passive wireless temperature sensor for harsh environment applications." *Sensors* 8, no. 12 (2008): 7982-7995.

[3] Franco, Alessandro, and Ana R. Diaz. "The future challenges for “clean coal technologies”: joining efficiency increase and pollutant emission control." *Energy* 34, no. 3 (2009): 348-354.

[4] Yvon, P., and F. Carré. "Structural materials challenges for advanced reactor systems." *Journal of Nuclear Materials* 385, no. 2 (2009): 217-222.

[5] Schueler, Martin, Christian Mandel, Margarita Puentes, and Rolf Jakoby. "Metamaterial inspired microwave sensors." *IEEE Microwave Magazine* 13, no. 2 (2012): 57-68.

[6] Childs, P. R. N., J. R. Greenwood, and C. A. Long. "Review of temperature measurement." *Review of scientific instruments* 71, no. 8 (2000): 2959-2978.

[7] Bentley, R. E. "The Theory and Practice of Thermoelectric Thermometry, Vol. 3 of Handbook of Temperature Measurement, edited by RE Bentley." (1998).

[8] Goldstein, R. J. "Optical measurement of temperature (Shadowgraph and interferometer systems for temperature measurements)." *1970.* (1970): 177-228.

[9] Adams, B. E. "Optical fiber thermometry for use at high temperatures." *Temperature: its measurement and control in science and industry* 6, no. 2 (1992): 739-744.

[10] Xiao, Hai, Jiangdong Deng, Gary Pickrell, Russell G. May, and Anbo Wang. "Single-crystal sapphire fiber-based strain sensor for high-temperature applications." *Journal of lightwave technology* 21, no. 10 (2003): 2276.

[11] Stevens, Daniel S., Jeffrey C. Andle, Sabah Sabah, Shravan J. Jumani, Bert WA Wall, Marcus Baier, Thomas Martens, and R. Gruenwald. "Applications of wireless temperature measurement using saw resonators." In *Fourth International Symposium on Acoustic Wave Devices for Future Mobile Communication Systems, Chiba University, Japan*. 2010.

[12] Sardini, E., and M. Serpelloni. "High-temperature measurement system with wireless electronics for harsh environments." In *Sensors Applications Symposium (SAS), 2011 IEEE*, pp. 256-261. IEEE, 2011.

[13] Whatmore, R. W. "Pyroelectric devices and materials." *Reports on progress in physics* 49, no. 12 (1986): 1335.

[14] Hossain, Akram, and Muhammad H. Rashid. "Pyroelectric detectors and their applications." IEEE Transactions on industry applications 27, no. 5 (1991): 824-829.

[15] Brownridge, James D., and Sol Raboy. "Pyroelectric response in LiNbO3 and LiTaO3 to temperature changes." *arXiv preprint physics/0107046* (2001).

[16] Srinivasan, M. R. "Pyroelectric materials." *Bulletin of Materials Science* 6, no. 2 (1984): 317-325.

[17] Yang, Ya, Wenxi Guo, Ken C. Pradel, Guang Zhu, Yusheng Zhou, Yan Zhang, Youfan Hu, Long Lin, and Zhong Lin Wang. "Pyroelectric nanogenerators for harvesting thermoelectric energy." *Nano letters* 12, no. 6 (2012): 2833-2838.

[18] Kohli, M., C. Wuethrich, K. Brooks, B. Willing, M. Forster, P. Muralt, N. Setter, and P. Ryser. "Pyroelectric thin-film sensor array." *Sensors and Actuators A: Physical* 60, no. 1 (1997): 147-153.

[19] Takenaka, Tadashi, K. Oichiro Sakata, and K. Ohji Toda. "Piezoelectric properties of (Bi1/2Na1/2) TiO3-based ceramics." *Ferroelectrics* 106, no. 1 (1990): 375-380.

[20] Lang, Sidney B. "Pyroelectricity: from ancient curiosity to modern imaging tool." *Physics today* 58, no. 8 (2005): 31.

[21] Terasaki, Ichiro, Yoshitaka Sasago, and Kunimitsu Uchinokura. "Large thermoelectric power in NaCo 2 O 4 single crystals." *Physical Review B* 56, no. 20 (1997): R12685.

[22] Odon, Andrzej. "Processing of signal of pyroelectric sensor in laser energy meter." *Measurement Science Review* 1 (2001): 215-218.

[23] Karim, Hasanul, Md Rashedul H. Sarker, Shaimum Shahriar, Mohammad Arif Ishtiaque Shuvo, Diego Delfin, Deidra Hodges, Tzu-Liang Bill Tseng, David Roberson, Norman Love, and Yirong Lin. "Feasibility study of thermal energy harvesting using lead free pyroelectrics." *Smart Materials and Structures* 25, no. 5 (2016): 055022.

[24] Navid, Ashcon, and Laurent Pilon. "Pyroelectric energy harvesting using Olsen cycles in purified and porous poly (vinylidene fluoride-trifluoroethylene)[P (VDF-TrFE)] thin films." *Smart Materials and Structures* 20, no. 2 (2011): 025012.

[25] Lee, Felix Y., Ashcon Navid, and Laurent Pilon. "Pyroelectric waste heat energy harvesting using heat conduction." *Applied thermal engineering* 37 (2012): 30-37.

[26] Batra, Ashok K., Sudip Bhattacharjee, Ashwith Kumar Chilvery, Mohan D. Aggarwal, Matthew E. Edwards, and Amar Bhalla. "Simulation of energy harvesting from roads via pyroelectricity." *Journal of Photonics for Energy* 1, no. 1 (2011): 014001-014001.

[27] Sebald, Gael, Daniel Guyomar, and Amen Agbossou. "On thermoelectric and pyroelectric energy harvesting." *Smart Materials and Structures* 18, no. 12 (2009): 125006.

[28] Cuadras, A., M. Gasulla, and Vittorio Ferrari. "Thermal energy harvesting through pyroelectricity." *Sensors and Actuators A: Physical* 158, no. 1 (2010): 132-139.

[29] Muralt, Paul. "Micromachined infrared detectors based on pyroelectric thin films." *Reports on Progress in Physics* 64, no. 10 (2001): 1339.

[30] Ivill, Mathew, Eric Ngo, and Melanie W. Cole. *Method and Characterization of Pyroelectric Coefficients for Determining Material Figures of Merit for Infrared (IR) Detectors*. No. ARL-TR-6758. ARMY RESEARCH LAB ABERDEEN PROVING GROUND MD WEAPONS AND MATERIALS RESEARCH DIRECTORATE, 2013.

[31] Hartley, N. P., P. T. Squire, and E. H. Putley. "A new method of measuring pyroelectric coefficients." *Journal of Physics E: Scientific Instruments* 5, no. 8 (1972): 787.

[32] Chynoweth, A. G. "Dynamic method for measuring the pyroelectric effect with special reference to barium titanate." *Journal of applied physics* 27.1 (1956): 78-84.

[33] Newsome, R. W., and E. Y. Andrei. "Measurement of the pyroelectric coefficient of poly (vinylidene fluoride) down to 3 K." Physical Review B 55, no. 11 (1997): 7264.

[34] Dias, C., M. Simon, R. Quad, and D. K. Das-Gupta. "Measurement of the pyroelectric coefficient in composites using a temperature-modulated excitation." *Journal of Physics D: Applied Physics* 26, no. 1 (1993): 106.

[35] Lang, Sidney B., and F. Steckel. "Method for the measurement of the pyroelectric coefficient, dc dielectric constant, and volume resistivity of a polar material." *Review of Scientific Instruments* 36, no. 7 (1965): 929-932.

[36] Simhony, M., and A. Shaulov. "Measurement of the pyroelectric coefficient and permittivity from the pyroelectric response to step radiation signals in ferroelectrics." *Applied Physics Letters* 21, no. 8 (1972): 375-377.

[37] Byer, Robert L., and C. B. Roundy. "Pyroelectric coefficient direct measurement technique and application to a nsec response time detector." *Ferroelectrics* 3, no. 1 (1972): 333-338.

[38] Gregory, Otto J., and Tao You. "Ceramic temperature sensors for harsh environments." *IEEE sensors journal* 5, no. 5 (2005): 833-838.

[39] Seifert, F., and R. Weigel. "SAW-based radio sensor and communication techniques." In *Microwave Conference, 1997. 27th European*, vol. 2, pp. 1323-1346. IEEE, 1997.

[40] Shi, Yongming, Yao Wang, Yuan Deng, Hongli Gao, Zhen Lin, Wei Zhu, and Huihong Ye. "A novel self-powered wireless temperature sensor based on thermoelectric generators." *Energy Conversion and Management* 80 (2014): 110-116.

[41] Lang, Sidney B., Steven A. Shaw, Lynn H. Rice, and K. D. Timmerhaus. "Pyroelectric thermometer for use at low temperatures." *Review of Scientific Instruments* 40, no. 2 (1969): 274-284.

[42] Tsai, C. F., and Ming-Shing Young. "Pyroelectric infrared sensor-based thermometer for monitoring indoor objects." *Review of Scientific Instruments*74, no. 12 (2003): 5267-5273.

[43] Smith, Brian, and Cristina Amon. "Simultaneous electrothermal test method for pyroelectric microsensors." *Journal of Electronic Packaging* 129, no. 4 (2007): 504-511.

[44] Batra, Ashok K., and Mohan D. Aggarwal. *Pyroelectric Materials: Infrared Detectors, Particle Accelerators and Energy Harvesters*. SPIE Press, 2013.

[45] Süli, Endre, and David F. Mayers. *An introduction to numerical analysis*. Cambridge university press, 2003.

[46] Sarker, Md Rashedul H., Hasanul Karim, Ricardo Martinez, Diego Delfin, Rodrigo Enriquez, Mohammad Arif Ishtiaque Shuvo, Norman Love, and Yirong Lin. "Temperature measurements using a lithium niobate ($LiNbO_3$) pyroelectric ceramic." *Measurement* 75 (2015): 104-110.

[47] Sarker, Md Rashedul H., Hasanul Karim, Ricardo Martinez, Norman Love, and Yirong Lin. "A Lithium Niobate High-Temperature Sensor for Energy System Applications." *IEEE Sensors Journal* 16, no. 15 (2016): 5883-5888.

[48] Savage, A. "Pyroelectricity and spontaneous polarization in $LiNbO_3$." *Journal of Applied Physics* 37, no. 8 (1966): 3071-3072.

[49] Bartholomäus, T., K. Buse, C. Deuper, and E. Krätzig. "Pyroelectric coefficients of $LiNbO_3$ crystals of different compositions." *physica status solidi (a)* 142, no. 1 (1994): K55-K57.

[50] Çengel, Yunus A., and Afshin Jahanshahi Ghajar. *Heat and mass transfer: fundamentals & applications*. McGraw-Hill, 2011

APPENDIX

Sample temperature calculation with $LiNbO_3$ wired sensor:

$$T_f = -\frac{1}{pA}\int_{t_i}^{t_f} Idt + T_i$$

T_i is the initial temperature. Room temperature was considered for initial temperature. T_f is the final temperature. Total amount of current for a certain time interval t_i to t_f was calculated by Simpson's one third rule.

T_i = 25.13 °C
p = - 8.5x10^{-5} C/m^2 °C ($LiNbO_3$ @ 25 °C)
A = 10^{-4} m^2
t_i = initial time = 1.6 s
t_f = final time = 7 s
I_i = initial current at corresponding time t_i = 0 A.
I_f = final current at corresponding time t_f = 5.21x10^{-10} A.

Total amount of current, $\int_{t_i}^{t_f} Idt = \left(\frac{t_f - t_i}{6}\right)\left(I_i + 4\frac{I_i + I_f}{2} + I_f\right)$ = 7.70x10^{-10} A (Simpson's one-third rule)

Final Temperature, $T_f = -\frac{1}{pA}\int_{t_i}^{t_f} Idt + T_i$ = 25.22 °C

Sample temperature calculation with PZT wireless sensor:

$$T_f = -\frac{1}{pA}\int_{t_i}^{t_f} Idt + T_i = -\frac{1}{pAC}\int_{t_i}^{t_f} Bdt + T_1$$

T_i is the initial temperature. Room temperature was considered for initial temperature. T_f is the final temperature. Total amount of magnetic field for a certain time interval t_i to t_f was calculated by Simpson's one third rule. C is the constant from all the physical parameters of the electromagnet, Table 2.2.

T_i = 23.40 °C

p = - 35x10^{-5} C/m^2 °C (PZT @ 25 °C)

A = 10^{-4} m^2

t_i = initial time = 0

t_f = final time = 1 s

B_i = initial magnetic field at corresponding time t_i = 0 T.

B_f = final magnetic field at corresponding time t_f = 7.5x10^{-13} T.

Total amount of magnetic field, $\int_{t_i}^{t_f} Bdt = \left(\frac{t_f - t_i}{6}\right)\left(B_i + 4\frac{B_i + B_f}{2} + B_f\right)$ (Simpson's one-third rule)

Final temperature, $T_f = -\frac{1}{pA}\int_{t_i}^{t_f} Idt + T_i = -\frac{1}{pAC}\int_{t_i}^{t_f} Bdt + T_1$ = 23.42 °C

VITA

Md Rashedul Hasan Sarker was born in January 1st 1985 in Dhaka, Bangladesh. He is the third child of Late Md Habibullah Sarker and Mrs. Meher Nigar. He is married to Rubaya Rabab. Mr. Sarker completed his Higher Secondary School from Government Science College, Dhaka, Bangladesh in 2001. His Bachelor of Science in Mechanical Engineering was awarded to him from Khulna University of Engineering and Technology, Bangladesh in 2007. Mr. Sarker graduated with his Master of Science degree in Mechanical Engineering from the University of Texas at El Paso in 2012. His thesis was entitled "Investigation on a Gas-Solid Fluidized Bed Hydrodynamics using a Non-Intrusive Technology to Visualize Flow Field". In august 2012, he enrolled in the Engineering Doctoral Program working towards his PhD in Mechanical Engineering. Mr. Sarker directly worked under supervision of Dr. Norman Love for developing wireless temperature sensor for high temperature applications. His dissertation title is "Investigation on Pyroelectric Ceramic Temperature Sensors for Energy System Applications". While working on his PhD he has published several articles related to his research, which spans the general topic of energy as applied to power generation systems.

Permanent Address: 29/1-B, Malibag Chowdhurypara
DIT Road, Dhaka-1219

This dissertation was typed by Md Rashedul Hasan Sarker.